Stable-isotope (H, O, and Si) evidence for seasonal variations in hydrology and Si cycling from modern waters in the Nile Basin: implications for interpreting the Quaternary record

H.E. Cockerton[a*], F.A. Street-Perrott[a], M.J. Leng[b,c], P.A. Barker[d], M.S.A. Horstwood[c], V. Pashley[c]

[a] Department of Geography, College of Science, Swansea University, Singleton Park, Swansea, SA2 8PP, United Kingdom
[b] Department of Geology, University of Leicester, Leicester, LE1 7RH, United Kingdom
[c] NERC Isotope Geosciences Laboratory, British Geological Survey, Keyworth, Nottingham, NG12 5GG, United Kingdom
[d] Lancaster Environment Centre, Lancaster University, Lancaster, LA1 4YQ, United Kingdom
* Corresponding author : Phone: +44 (0)1792 295531 ; E-mail: h.cockerton.292399@swansea.ac.uk

Keywords: hydrological cycle, silicon cycle, palaeoclimatology, oxygen isotopes, silicon isotopes, diatoms

Abstract

Seasonal variations in hydrology and Si cycling in the Nile Basin were investigated using stable-isotope (H, O, and Si) compositions and dissolved Si (DSi) concentrations of surface waters, as a basis for interpreting lacustrine diatom sequences. $\delta^{18}O$ ranged from –4.7 to +8.0‰ in the wet season and +0.6 to +8.8‰ in the dry season (through 2009-2011). Higher $\delta^{18}O$ values during the dry season reflected increased evapotranspiration and open-water evaporation under conditions of lower humidity. Progressive downstream enrichment in the heavy isotope ^{18}O also occurred in response to cumulative evaporative losses from open water bodies and swamps. $\delta^{30}Si$ values of DSi ranged from +0.48 to +3.45‰ during the wet season and +1.54 to +4.66‰ during the dry season, increasing the previously reported global upper limit for $\delta^{30}Si$ values in natural waters by 1‰. Si-isotope fractionation was most intense during the dry season when demand for DSi by aquatic ecosystems exceeded supply. Progressive downstream enrichment in the heavy isotope ^{30}Si, coupled with decreasing DSi concentrations, represented cumulative Si uptake by diatoms, macrophytes and other Si-accumulating aquatic organisms. The pronounced seasonal variations in DSi concentrations and Si-isotope compositions in the River Nile suggest that its DSi flux to the ocean may have varied significantly on a glacial/interglacial time scale, with important consequences for the marine Si budget and consequently the global C cycle. Anthropogenic impacts were evident in both the water- and Si-isotope datasets, especially during the dry season and along the Main Nile, where water management is most intensive.

1 Introduction

Variations in the stable-isotope composition of surface waters are valuable tracers of the hydrological cycle (O and H isotopes) and the Si cycle (Si isotopes), both for the modern system and for palaeoenvironmental studies (Kendall and Coplen, 2001; Georg et al., 2006a; Street-Perrott and Barker, 2008; Street-Perrott et al., 2008). When interpreting stable-isotope data from the sediment record it is essential to understand the isotope systematics of the modern system in order to identify the factors that influenced the isotopic composition of the sediment archive (Leng and Marshall, 2004). Diatoms, photosynthetic microalgae found in most aquatic environments, are typically well preserved and abundant in lacustrine sediments (Round et al., 1990). Diatom silica is formed of biogenic opal ($SiO_2 \cdot nH_2O$) containing oxygen and silicon isotopes that can be used in palaeoenvironmental studies (Leng and Barker, 2006; Leng and Swann, 2010). The isotopic composition of the frustules reflects the aqueous environment in which they formed. The oxygen-isotope composition of diatoms ($\delta^{18}O_{diatom}$) is controlled primarily by water temperature and/or by the isotope composition of the water, whereas their silicon-isotope composition ($\delta^{30}Si_{diatom}$) is related to the availability of this nutrient, which in turn is connected to local factors such as catchment geology and vegetation, chemical weathering, river and groundwater inputs, water-residence time and the occurrence of seasonal diatom blooms (Leng and Marshall, 2004; Leng and Barker, 2006; Leng et al., 2009).

Surface waters can be valuable indicators of the average isotopic composition of rainfall, especially in situations in which limited evaporative enrichment has occurred since precipitation (Fritz, 1981). The linear relationship between δ^2H and $\delta^{18}O$ in meteoric waters was established by Craig (1961) as $\delta^2H = 8 \cdot \delta^{18}O + 10‰$, and is known as the Global Meteoric Water Line (GMWL), although local deviations due to differing climatic and geographical factors (Clark and Fritz, 1997). Hence, in regional or site-specific studies, a Local Meteoric Water Line (MWL) may be preferred. Globally, variations in the δ^2H and $\delta^{18}O$ ratios of precipitation are controlled by climatic (temperature, rainfall amount, humidity, evaporation, wind regime) and geographical parameters (latitude, altitude, distance from moisture source) as described by Dansgaard (1964). At low latitudes, the spatial distribution of isotopes in precipitation is primarily controlled by the source of the water, subsequently modified by continental, altitude and amount effects that are explained by the Rayleigh distillation process. Along the trajectory of an air mass, isotopically heavy water molecules preferentially fall from a diminishing vapour mass, leaving the residual vapour to become progressively depleted (leading to lower δ^2H and $\delta^{18}O$). Subsequent rainfall becomes increasingly lower in isotopic composition (Dansgaard, 1964; Clark and Fritz, 1997; Gat, 1996, 2000). This rain-out effect occurs during the transport of an air mass from an oceanic

moisture source to the interior of a landmass (continental effect), during orographic uplift (altitude effect) and during heavy convective rainstorms such as those associated with the passage of the Intertropical Convergence Zone (ITCZ) (amount effect).

Deviation from the GMWL/MWL indicates that kinetic effects have modified the original isotopic composition of the precipitation since it was formed. Several processes can cause this effect. Surface water or rainfall that has undergone evaporation will typically plot below the MWL on independent Local Evaporation Lines (LELs) (Craig, 1961; Gat et al., 1994). Low humidity leads to slopes very different from the MWL as water-vapour exchange is minimized, and evaporation becomes an increasingly non-equilibrium (kinetic) process, leaving the residual water enriched in the heavier isotopes ^{18}O and ^{2}H (Craig and Gordon, 1965). Rain condensed from this evaporated vapour will plot above the MWL (i.e. with a greater y-intercept, or deuterium excess). The concept of deuterium excess (or d-excess), defined as d (‰) = $\delta^{2}H - 8 \cdot \delta^{18}O$, was introduced by Dansgaard (1964). It measures the degree of evaporation at the moisture source or the amount of evaporative enrichment in ^{18}O after the water has condensed. The most important control on d-excess is thought to be humidity (Merlivat and Jouzel, 1979). Information about the fractionating processes in convective systems can be obtained from d-excess values, which may have been modified from their original source composition during their transportation to the precipitation site (Fröhlich et al., 2002). Values lower than 10‰ may indicate secondary evaporation processes, such as the evaporation of falling raindrops in a warm, dry atmosphere (Stewart, 1975; Araguás-Araguás et al., 2000). Recycling of water vapour in continental basins may be responsible for large d-excess values, as identified in the Amazon Basin (Gat and Matsui, 1991) and the Great Lakes region of North America (Gat et al., 1994).

Growing interest in the role of continental biota in the global Si cycle reflects the close coupling between the global biogeochemical cycles of Si and C (see Street-Perrott and Barker (2008) and Struyf et al. (2009) for reviews). Previously, the main focus was on long-term geological processes of silicate-rock weathering and the drawdown of CO_2 in the marine realm (Berner et al., 1983; Berner, 1994, 1995; Smetacek, 1998; Dugdale and Wilkerson, 2001; Yool and Tyrrell, 2003; Ragueneau et al., 2006; Hilley and Porder, 2008). However, growing evidence shows that certain plants and aquatic organisms have the ability to modify the Si cycle by taking up, recycling and storing significant amounts of Si in their cells before it reaches the ocean (Conley, 1997, 2002; Street-Perrott and Barker, 2008; Struyf and Conley, 2009). Although Si is not classified as an essential nutrient for plants, amongst other benefits, it can enhance structural rigidity and growth, and reduce abiotic and biotic stresses (Raven, 1983; Jones and Handreck, 1967; Epstein, 1999; Ma et al., 2001).

Certain plants that contain >1% dry weight of silica are known as Si accumulators. These are abundant in a variety of terrestrial and aquatic ecosystems (e.g. grasslands, tropical rainforests, temperate deciduous forests and wetlands). They have the potential to retain large amounts of Si (Bartoli, 1983; Alexandre et al., 1997; Struyf et al., 2005; Blecker et al., 2006; Struyf et al., 2007; Street-Perrott and Barker, 2008; Struyf and Conley, 2009; Schoelynck et al., 2010; Alexandre et al., 2011).

Si is ultimately derived from silicate-rock weathering and is released in dissolved form (dissolved Si; DSi) as orthosilicic acid ($Si(OH)_4$. Globally, weathering rates are high in tropical headwaters where high relief, high annual-mean temperatures and monsoonal rainfall facilitate rapid physical weathering and erosion, creating freshly weathered surfaces and thereby enhancing the rate of chemical weathering (Brady and Carroll, 1994; White and Blum, 1995; Cochran and Berner, 1996; Gaillardet et al., 1999). In addition to the effects of bedrock composition, topography and climate, it has been shown that higher plants accelerate the rate of silicate weathering by improving the moisture and organic-matter status of soils (Hinsinger et al., 2001). Interactions between plant roots and soil microbes in the rhizosphere also expedite chemical weathering (Kelly et al., 1998; Lucas, 2001).

DSi present in soil solution may be taken up by terrestrial vegetation and precipitated as hydrated amorphous silica (phytoliths), or transported into rivers and lakes, where Si-accumulating aquatic organisms, such as diatoms, sponges and aquatic macrophytes, progressively extract DSi. The residual DSi is transported via rivers, eventually reaching the oceans where it is an essential nutrient for the siliceous phytoplankton that dominate the marine biological pump (Harrison, 2000; Tréguer and Pondaven, 2000). On glacial to interglacial time scales, the Si flux to the oceans can therefore be expected to vary as a result of changes in climate, vegetation type and distribution, hydrology and limnology (Georg et al., 2006a; Street-Perrott and Barker, 2008; Engström et al., 2010).

Although measurements of Si isotopes in natural samples are still relatively scarce, previously reported $\delta^{30}Si$ values for fresh waters range from –0.17 to +3.4‰ (De La Rocha et al., 2000; Ding et al., 2004; Alleman et al., 2005; Georg et al., 2006a; Georg et al., 2007; Georg et al., 2009; Cardinal et al., 2010; Engström et al., 2010; Ding et al., 2011; Opfergelt et al., 2011; Hughes et al., 2012), showing that DSi in rivers and lakes is isotopically heavy compared with primary minerals (felsic magmatic rocks: $\delta^{30}Si = –0.07 \pm 0.05$‰; gneisses, granulites and migmatites: $\delta^{30}Si = –0.10 \pm 0.15$‰ (André et al., 2006); and mafic magmatic rocks: $\delta^{30}Si = –0.29 \pm 0.08$‰ (Savage et al., 2011)). During formation of secondary products (e.g. phytoliths, diatoms and clays), the light isotope of Si (^{28}Si) is preferentially incorporated

into the product (De La Rocha et al., 2000), thereby enriching the residual aqueous solution in the heavier isotopes ^{29}Si and ^{30}Si. Hence, Si isotopes offer great potential as tracers of the continental Si cycle (Street-Perrott and Barker, 2008).

Although several studies have used Si isotopes to trace Si cycling in a few river basins across the globe (Ding et al., 2004; Georg et al., 2006a; Georg et al., 2007; Georg et al., 2009; Cardinal et al., 2010; Engström et al., 2010; Ding et al., 2011; Hughes et al., 2012), no-one has so far investigated downstream Si cycling under different climatic regimes in a basin-wide study. Here, we present an overview of the first downstream dataset of coupled δ^2H, $\delta^{18}O$ and $\delta^{30}Si$ measurements on surface waters, in order to determine the impact of seasonal hydrological changes on Si cycling in the Nile Basin. Understanding the processes controlling the isotope systematics of surface waters will facilitate interpretation of the lacustrine diatom record from river-fed lakes along the River Nile.

2 Regional Setting

2.1 Geography

The Nile Basin covers an area of over 3 million km^2 across ten countries and has a length of about 6700 km, making it the longest river in the world. The catchment extends from 4°S to 32°N, spanning a wide variety of altitudinal, geological, geomorphological, climatic and vegetation zones (Figs. 1 and 2). The main tributaries are the White Nile, originating from the headwaters of the equatorial great lakes in East Africa, and the Blue Nile and Atbara which descend from the Ethiopian Highlands. The two Niles converge in Khartoum, Sudan, and flow northwards to the Mediterranean Sea. Climate and vegetation are closely correlated with precipitation amount and the number of dry months, which are primarily governed by the northward migration of the ITCZ in boreal summer, and by orography (Nicholson, 1996) (Fig. 2).

2.2 Geology

The White Nile and Blue Nile are geologically distinct (Fig. 2a). A large portion of the Nile Basin is underlain by Precambrian granitic and metamorphic rocks. Volcanic rocks are more extensively developed in Ethiopia than anywhere else along the East African Rift system (Williams et al., 2006; Schlüter, 2008). Although the Blue Nile Basin is underlain by Precambrian crystalline basement, over two-thirds of the Upper Blue Nile Basin is covered by a thick stack of weathered trap basalts (Kebede et al., 2005). The Atbara passes through a similar succession of rock types. In the headwaters of the White Nile, small pockets of

volcanics occur along the Western Rift (e.g. Virunga Mountains) and east of Lake Victoria. However, more than two-thirds of Uganda are underlain by Precambrian granites, granulites and gneissic sequences that continue further downstream into the western part of the Sudd and the Bahr el Ghazal. From Juba northwards along the main channel and in the plains in the east, unconsolidated sediments are widespread. In northern Sudan and southern Egypt, the Main Nile flows over continental clastic sequences and crystalline basement rocks. The remainder of its passage to the Delta crosses unconsolidated marine sediments.

2.3 Climate

Temporal variations in the hydrological budget of the River Nile are largely governed by the seasonal migration of the Intertropical Convergence Zone (ITCZ), which separates the relatively stable, northeast monsoon from southeasterly monsoon airflow from the Indian Ocean, and moves north and south across the Equator following the overhead sun (Fig. 2b). The Congo Air Boundary (CAB) defines the convergence of unstable, moist westerly flow from the Atlantic Ocean and easterly flow from the Indian Ocean (Nicholson, 1996). The passage of the ITCZ usually coincides with maximum rainfall due to intensified convective activity; as a result, the equatorial regions of the White Nile exhibit a bimodal rainfall pattern (Fig. 2c). In the headwaters of both the White and Blue Niles, mean annual rainfall exceeds 1000mm/year, with additional factors such as topography and continental water bodies (notably the equatorial great lakes and Lake Tana) having an influence on regional and local climates through the distribution of orographic precipitation, rain shadows and land-lake circulations (Nicholson, 1996). In contrast, northern Sudan (from ~18°N) and Egypt, which lie well beyond the maximum northward limit of the ITCZ (Fig. 2c), experience negligible rainfall (<50 mm annually) (Camberlin, 2009). In summary, a very pronounced south-to-north gradient of decreasing rainfall and increasing total number of dry months characterizes the Nile Basin.

2.4 Hydrology

The White Nile flows northwards from the equatorial lakes plateau (Lakes Victoria, Edward, George and Albert) through a series of lakes and swamps. The western (Rwenzori Mountains, Lake Edward, River Semliki and Lake Albert) and eastern (Lake Victoria, Lake Kyoga and Victoria Nile) branches of the White Nile meet at the northern end of Lake Albert to form the Albert Nile (Fig. 1). From Uganda, the White Nile flows into South Sudan as the Bahr el Jebel and enters vast wetlands (30,000-40,000 km^2) known as the Sudd, where the river spills over from the main channel into swamps and seasonal grasslands; only about half the inflow is returned to the main channel as a result of evaporative losses (Sutcliffe and

Parks, 1999; Mohamed et al., 2005). Beyond the Sudd, the Bahr el Ghazal enters from the west, although its contribution to the Nile is negligible due to evaporation and overspill. The Sobat, which drains the south-western Ethiopian Highlands and the South Sudan Plains, is the final tributary to enter the White Nile, contributing about half the total flow (Sutcliffe and Parks, 1999).

The White Nile, fed by more consistent year-round rainfall in the equatorial lakes region, contributes a smaller proportion (~30%) of the total Nile flow but a more constant discharge throughout the year than the Blue Nile (Hurst, 1952; Foucault and Stanley, 1989). Its seasonal variations in flow are also dampened by storage in major lakes, reservoirs and wetlands (Green and El-Moghraby, 2009). In contrast, the Blue Nile descends from Lake Tana (3156 km^2, 1,800 m a.s.l.) in the western Ethiopian Highlands (average ~2000-3000 m a.s.l., rising to >4000 m) and contributes about 56% of the Main Nile flow (Foucault and Stanley, 1989). Lake Tana alone supplies ~8% of the main river flow, the remainder coming from tributaries draining the central and southwestern Blue Nile basin (Shahin, 1985; Conway, 2000). Near Roseires, at the Ethiopian-Sudan border, the river drops steeply down to the plains of Sudan (<700 m) before flowing northwestwards towards Khartoum (Shahin, 1985; Sutcliffe and Parks, 1999). The highly seasonal flow of the Blue Nile reflects the unimodal rainfall regime at this latitude (Fig. 2c). Its sediment load is also very high (72% of total Nile sediment load), due to the steep slopes and relatively sparse vegetation of the Ethiopian Highlands (Foucault and Stanley, 1989; Sutcliffe and Parks, 1999). Downstream from the confluence, the Main Nile flows northwards through ~3000 km of desert, with its final tributary, the Atbara, joining 300 km north of Khartoum. The Atbara drains the northern Ethiopian Highlands and parts of Eritrea. It has an even more flashy flow regime than the Blue Nile, due to its proximity to the northern summer limit of the ITCZ, though it still provides ~14% of the total Nile flow (Foucault and Stanley, 1989). Below the confluence with the Atbara, several major dams, including the new Merowe Dam and the older High and Low Dams at Aswan, regulate the flow and store summer flood waters for hydroelectric power and irrigation, thereby enhancing evaporation losses (Abu-Zied and El-Shibini, 1997). Lake Qarun, near Cairo, is a closed lake fed by a major irrigation canal from the Main Nile.

2.5 Vegetation

The large-scale pattern of natural vegetation and plant biomass in the Nile drainage reflects the northward decrease in mean annual rainfall, topography and the distribution of surface water bodies (Fig. 2d). Biomass decreases northwards in the Nile Basin following the rainfall gradient (Fig. 2). Surrounding the equatorial lakes (e.g. Victoria, Kyoga, George, Edward

and Albert) and Lake Tana are extensive wetlands composed of aquatic grasses, large sedges and floating and submerged macrophytes (Langdale-Brown et al., 1964; Kendall, 1969; Conway, 1997; Sutcliffe and Parks, 1999; Green, 2009; Green and El-Moghraby, 2009). In addition, the main river channels and many of their tributaries are lined with swamps and small ponds, including the vast areas of the Sudd and Bahr el Ghazal swamps (the area of the latter is uncertain but smaller than the Sudd) (Sutcliffe and Parks, 1999). Terrestrial vegetation along the Main Nile from about 18°N is very sparse, consisting mainly of acacia bush and doum palms, although the banks of the Nile are fringed by riparian swamps and irrigated fields.

3 Methodology

3.1 *Sampling*

A total of 79 water samples was collected along the White, Blue and Main Nile drainages, including major tributaries and lakes, during both low-flow ("dry season": May-June 2009 and April-May 2011) and high-flow conditions ("wet season": October-December 2010), in order to represent seasonal variations (Fig. 1, Table 1). Samples were collected in pre-cleaned HDPE bottles from freely following water. In the field, they were filtered through 0.45µm Millipore™ cellulose nitrate filters to remove particulate Si (including biogenic silica), as well as suspended organic matter, and acidified with ultra-pure HCl to a pH of between 2 and 3 to prevent any further biological activity or polymerization (Georg et al., 2006b). They were stored in clean 250ml HDPE bottles, and where possible, in dark and cool conditions whilst in the field. Air was evacuated by simply squeezing each bottle and allowing the contents to overflow before sealing it with a screw lid. On return to the UK, samples were stored at ~4ºC until further analysis analysed for H, O and Si isotopes at the NERC Isotope Geosciences Laboratory, British Geological Survey, UK. It should be noted that due to logistical and financial constraints, dry-season samples for the Upper and Lower Nile were collected two years apart and therefore do not reflect continuous sampling down the length of the river during a single dry season. Unfortunately political instability prevented travel through South Sudan, thereby ruling out sampling of the Sudd and Bahr el Ghazal swamps, which are believed to play important roles in both the hydrological (Sutcliffe, 1974), and Si cycles (McCarthy et al., 1989; Cardinal et al. 2010).

3.2 Isotope analysis

For oxygen-isotope analysis, the waters were equilibrated with CO_2 using an Isoprep 18 device, mass spectrometry being performed on a VG SIRA. For hydrogen-isotope analysis, an on-line Cr reduction method was used with a EuroPyrOH-3110 system coupled to a Micromass Isoprime mass spectrometer. Isotopic ratios ($^{18}O/^{16}O$ and $^{2}H/^{1}H$) are expressed in standard delta notation, as $\delta^{18}O$ and $\delta^{2}H$ (‰, parts per mille), with respect to the international standard VSMOW (Vienna Standard Mean Ocean Water). Analytical precision was typically $\pm$0.05‰ for $\delta^{18}O$ and $\pm$1.0‰ for $\delta^{2}H$.

Quantification of Si concentrations and total cation content was carried out on an Agilent 7500cx series quadrupole ICP-MS with an octopole reaction system (ORS) (Si precision ± 15%). NBS-28 (NIST RM 8546) and Diatomite reference materials were prepared by grinding in an alumina pestle and mortar prior to fusing 1-10mg of sample with 200mg Merck Suprapur NaOH at 720^{o}C for 30mins in a homemade Ag crucible. The resulting 'fusion cake' was dissolved in 20ml deionised (Milli-Q) H_2O within a cleaned Savillex vial. The reference materials were stored in a pre-cleaned FEP bottle and diluted for storage using Milli-Q H_2O. Prior to Si-isotope analysis, all 41 samples and reference materials were purified using cation-exchange chromatography in a class 100 clean suite following methods of Georg et al. (2006b) and van den Boorn et al. (2006). Samples were loaded onto 1.8ml Bio-Rad® AG 50W-X12 resin in a 10ml Bio-Rad® column. Column cleaning was performed following Georg et al (2006b). The pH of the final cleaning elutant was checked prior to loading and eluting the sample into a pre-cleaned Savillex vial using 3ml Milli-Q H_2O. Samples were then individually diluted to a desired concentration where appropriate and stored at ~4^{o}C. Prior to analysis each sample was centrifuged at 3,000rpm for 10 minutes and filtered using an inert Ezee filter (sintered polyethylene, 60-90µl frit size) and acidified using HCl (to a concentration of 0.05M, using twice quartz distilled acid), doped with sulphuric acid (to a concentration of 0.001M, using Romil Ultra Purity Acid) following the recommendations of Hughes et al (2011), as well as ~300ppb magnesium (Mg, Alfa Aesar SpectraPure). All samples, reference materials and blanks were made up equivalently to ensure matrix matching.

Silicon isotopes were determined using the high-resolution capacity of a Thermo Scientific Neptune Plus MC-ICP-MS operating in wet-plasma mode using a Meinhard 200ul/min glass nebuliser, nebuliser gas flow 1.17l/min, a stable sample introduction system quartz dual cyclonic spray chamber, a demountable torch with a sapphire injector and standard 'H' sample and skimmer interface cones. Sample uptake time was 90secs with a typical

washout time of ca.5mins. Using the instrumental parameters outlined, sensitivity of 6-11V/ppm was obtained with an instrument background contribution of ~0.4% (~45mV ^{28}Si measured on the blank acid). Data were acquired using a dynamic, two sequence acquisition method to collect first the Si and then the Mg, using a 16.8secs integration time for the Si and 8.4secs for the Mg with a 3secs settle time between each magnet jump. Faraday amplifier gains were measured at the beginning of each analytical session, with a 5 minute defocused instrument baseline measured daily. Data were collected in 1 block of 20 ratios, with a resulting analysis time of ~12 minutes per sample (including the sample uptake and stabilisation time). Blanks were measured on the sample make-up acid (0.05M HCl, 0.001M H_2SO_4) using a shortened version of the acquisition procedure above (i.e. 1 block of 10 ratios). An on-line background correction was made, with the values obtained for the blank acid subtracted from each succeeding sample.

The validation reference material (Diatomite) was analysed two to four times during each analytical session as a check on procedural accuracy. Data were corrected on-line for mass bias using an exponential function assuming $^{24}Mg/^{25}Mg = 0.126633$ and normalised to the external bracketing calibrator. Uncertainties were propagated to reflect the session repeatability (SD) of the external calibrator (NBS-28) after self-normalisation to correct for drift. Data are reported as delta values (δ) reflecting deviation from the delta-zero calibrator (NBS-28) in parts per thousand. The overall reproducibility of the NBS-28 reference material was ±0.15‰ for $\delta^{29}Si$, and ± 0.18‰ (2SD) for $\delta^{30}Si$ using calibrator concentrations equivalent to those of the river water samples (between 0.75 and 3ppm) resulting in a ^{30}Si ion beam intensity of 50-300mV. For the whole period over which the samples were analysed (a total of 9 sessions during a 1 month period) the validation results (Diatomite) were 0.64 ± 0.19‰ and 1.28 ± 0.26‰ (2SD), for $\delta^{29}Si$ and $\delta^{30}Si$ respectively, virtually identical to the values of Reynolds et al. (2007), despite analyses differing by a factor of four in their concentration (0.75 to 3ppm) (Table 2). All data followed the expected mass dependent fractionation line ($\delta^{29}Si = 0.5345 \cdot \delta^{30}Si - 0.039$, $R^2 = 0.962$). Six separate aliquots of sample 11 (R. Semliki) were purified and analysed to investigate analytical uncertainty on the samples. Total repeatability for these data was ± 0.20‰ and ± 0.19‰ (2SD), for $\delta^{29}Si$ and $\delta^{30}Si$ respectively.

4 Results

4.1 δ^2H and $\delta^{18}O$

All δ^2H and $\delta^{18}O$ values for surface water samples (Table 1) are plotted for the Nile drainage as a whole (Fig. 3a), and individually for the White (Fig. 3b), Blue (Fig. 3c) and Main (Fig. 3d)

Niles, with reference to the African Meteoric Water Line (AMWL) (solid line). The AMWL ($\delta^2H = 7.4 \cdot \delta^{18}O + 10.1$) represents the isotopic values of precipitation in the interior of East and Central Africa, and differs slightly from the GMWL (Cohen et al., 1997). The validity of using the AMWL is confirmed by the fact that small rivers draining into the main branches of the River Nile plot on or close to the AMWL. Sites deviating from the AMWL form local evaporative lines (LELs) which are shown for both wet- and dry-season conditions (Fig. 3, Table 3).

$\delta^{18}O$ values in the Nile Basin ranged from -4.7 to +8.0‰ in the wet season and +0.6 to +8.8‰ in the dry season (Fig. 3, Table 3). Dry-season samples (average $\delta^{18}O = +3.9 \pm 2.2$‰; n = 34) were significantly more enriched in ^{18}O than wet-season samples (average $\delta^{18}O = +0.8 \pm 2.9$‰; n = 45) (paired *t*-test, p = 0.001) (Figs. 3a, 4). However, there was no significant difference between the slopes of the LELs in different seasons in any of the individual sub-basins (Fig. 3b-d). Due to the complicated hydrography of the River Nile (i.e. many tributaries), latitude is used here as a convenient proxy for downstream distance. Each major sub-basin exhibited distinct δ^2H and $\delta^{18}O$ values, especially during the wet season, with both δ^2H and $\delta^{18}O$ values increased northwards and downstream (Figs. 3 and 4, Table 3). The $\delta^{18}O$ values for the Main Nile were significantly higher than those of either the White Nile (separate variance *t*-test, $p < 0.01$) or the Blue Nile (separate variance *t*-test, $p < 0.0001$) during the wet season, but no statistically significant differences in $\delta^{18}O$ values between basins were found for the dry season (Fig. 3, Table 3). Significant relationships were observed during the wet season between $\delta^{18}O$ and latitude (Fig. 4a; $r_s = 0.465$, $p < 0.001$) and $\delta^{18}O$ and altitude (Fig. 4b; $r_s = -0.724$, $p < 0.001$), although no significant trends were found in the dry season. Isotopically lower surface-water samples from high-altitude, headwater sites (Fig. 4) in the White Nile (Fig. 3b) and Blue Nile catchments (Fig. 3c) displayed large d-excess values compared with the GMWL (+10‰) (Fig. 5).

4.2 Dissolved Si concentrations and $\delta^{30}Si$

Dissolved Si concentrations (DSi) are displayed in both milligrams per litre (mg/L) and micromolar (µM) units in order to facilitate comparisons with published literature (Fig. 6, Table 1). µM values follow mg/L values in parentheses. Due to the contrasting geology in the individual sub-basins (Fig. 2a), regression lines for DSi have been plotted individually for both wet and dry seasons. Waters from the Ethiopian highlands (Blue Nile and Atbara catchments) had the highest DSi contents under both wet-season (average 10.3 ± 4.7 mg/L (365 ± 169 µM)) and dry-season conditions (average 5.7 ± 3.0 mg/L (204 ± 109 µM)), whereas White Nile waters contained roughly half as much Si (wet season: 5.2 ± 3.6 mg/L

(187 ± 127 μM); dry season: 3.7 ± 3.8 mg/L (133 ± 135 μM)) (Fig. 6). A northwards decrease in DSi was seen in all sub-basins during both seasons (Fig. 6). DSi concentrations were highest during the wet season, particularly in rivers draining the Ethiopian Highlands (Fig. 6).

The $\delta^{30}Si$ values for both wet- and dry-season datasets are best described by curvilinear regressions (Fig. 7). These curves reflect lower values in Nile headwaters, with progressive enrichment of ^{30}Si downstream, becoming more pronounced in the Main Nile (Fig. 7). $\delta^{30}Si$ values ranged from +0.48 to +3.45‰ during the wet season and +1.54 to +4.66‰ during the dry season, raising the upper limit of reported global $\delta^{30}Si$ values for DSi in natural waters by more than 1‰. All samples had high $\delta^{30}Si$ compositions relative to the local geology and were higher in the dry season (av. +2.79 ± 0.91‰) than during the wet season (av. +2.02 ± 0.72‰), although there was less seasonal contrast in the Main Nile (Fig. 7). $\delta^{30}Si$ and DSi were negatively correlated; low Si concentrations corresponded to high $\delta^{30}Si$ values, more so during the dry season (R^2 = 0.371; separate variance *t*-test, p = 0.012) than the wet season (R^2 = 0.058; separate variance *t*-test, p = 0.245) (Fig. 8). Fig. 9 shows a statistically strong, albeit non-causal, positive correlation between $\delta^{30}Si$ and $\delta^{18}O$ during the wet season (R^2 = 0.517; separate variance t-test, p < 0.001), when, as we have seen, both isotopic parameters became cumulatively enriched downstream (Figs. 4 and 7). However, there was no statistically significant relationship between $\delta^{30}Si$ and $\delta^{18}O$ during the dry season. In the following section, specific numbered sampling sites (enclosed in square brackets) correspond to Table 1 and Fig. 1.

5 Discussion

5.1 δ^2H and $\delta^{18}O$

Remarkably, all surface-water samples from the Nile drainage plotted along effectively the same evaporative line with a slope of about 5 (Fig. 3a), implying similar isotope systematics, including kinetic effects imparted during evaporation. Individual sampling sites migrated seasonally up and down the LELs representing their respective sub-basins (Fig. 3), yielding dry-season samples that were significantly higher in δ^2H and $\delta^{18}O$ than wet-season samples, as the combined result of increased evapotranspiration and evaporation losses under conditions of lower humidity.

The isotopically lowest values were obtained in the headwaters [1-7, 25-33] and the isotopically highest towards the Delta in Lake Qarun [48-50] (Figs. 3 and 4). Progressive downstream increases in both isotope ratios along the Nile are attributed mainly to cumulative evaporation losses from swamps and open water bodies, such as the Sudd, the

equatorial great lakes and slow moving branches of the River Nile. However, the composition of the waters also reflect the strong northwards decline in total rainfall and total number of wet months (Fig. 2c). Downstream increase was only significant during the wet season. The downstream increase in $\delta^{18}O$ was only significant during the wet season (Fig. 4). In contrast, the latitudinal trend was not well defined during the dry season when water-management practices such as irrigation and use of dams to control seasonal flow were more prevalent, most notably along the Main Nile (Fig. 4). For example, waters collected from east of Lake Tana [25, 30] in the Ethiopian Highlands had highly evolved $\delta^{18}O$ values during the dry season (Figs. 3c and 4), reflecting the use of irrigation in the intensively cultivated Fogera Plain (~500,000 ha) (World Bank, 2008), which is bounded by the Rivers Ribb [25] and Gumara [30]. Waters sampled from the Main Nile, close to Khartoum [41-42], were extremely enriched in ^{18}O compared to downstream sites (except for Lake Qarun which is hydrologically closed) [38-40, 43-47] but had a similar composition to the White Nile [13] upstream (Fig. 3), indicating a possible release of isotopically enriched waters from the Jebel Aulia Dam (~50 km south of Khartoum) on the White Nile (Fig. 1), shortly prior to sampling at Khartoum.

The corresponding lack of a significant altitudinal gradient in $\delta^{18}O$ during the dry season (Fig. 4b) can be explained by several factors: greater evaporative enrichment as a result of decreased humidity; active water management in the Tana headwaters and along the Main Nile; and sampling during more than one dry season. The altitudinal isotope gradient observed in River Nile waters during the wet season (–2.6‰ km^{-1}) was similar to the slope of rainfall samples from other tropical regions, which varied between –2.7 ± 0.3‰ km^{-1} and –1.6 ± 0.05‰ km^{-1} (Gonfiantini et al., 2001) as a result of progressive rainout of ^{18}O following a Rayleigh adiabatic condensation process. However, deviations from the average altitudinal gradient were seen at sub-basin scale in the Nile drainage (not shown here).

The most negative values of $\delta^{2}H$ and $\delta^{18}O$ were found at high-altitude sites in the headwaters of the White [1-7] and Blue [25-33] Niles during the wet season (Fig. 4). This is attributed to the combined effects of orographic enhancement and the very continental location with respect to oceanic moisture sources (Indian and Atlantic Oceans) (Fig. 1); both these effects are associated with progressive rainout of the heavier isotopes of hydrogen and oxygen, resulting in isotopically depleted rainfall. Evaporative enrichment at these sites is limited by the steep gradients of the rivers and high humidity during the wet season. In addition, these samples displayed large d-excess values (>10‰) (Fig. 5), indicating that they originated from rainfall that formed in part from recycled moisture (Gat and Matsui, 1991; Gat et al., 1994).

It has been recently shown that precipitation during the summer rainy season in western Ethiopia carries the isotopic imprint of recycled continental moisture transported by south-westerly and westerly flow from the Congo rainforest and the swamps of the Sudd (Levin et al., 2009; Kebede and Travi, 2012), supporting earlier work by Rozanski et al. (1996) and Sonntag et al. (1979). Kebede and Travi (2012) found that water samples from the Blue Nile Plateau had the highest d-excess values in their Ethiopian dataset, which they attributed to recycling of moisture through evapotranspiration and evaporation from open water, at both local and continental scales. While vegetation-controlled vapour loss (transpiration) is generally non-fractionating (Salati et al., 1979; Gat and Matsui, 1991; Gat et al., 1994), evaporation from soils and surface waters produces vapour with high d-excess values, resulting in subsequent rainfall with these characteristics.

In the northern Ethiopian Highlands during the rainy season, convective clouds tend to form at the end of the morning, as a result of daytime heating of the land, creating rain in the afternoon (Nyssen et al., 2005). Hence, evaporation from large surface water bodies (Gat et al., 1994), for example Lake Tana and its surrounding wetlands, are likely to be a significant source of recycled water vapour, resulting in precipitation and initial surface runoff with large d-excess values. Similarly, over Lake Victoria (68,000 km^2), the largest lake in Africa, rainfall is enhanced by a strong nocturnal land-lake breeze (Flohn and Fraedrich, 1966); the prevailing south-easterly trade winds play an important role by displacing the centre of night-time convergence towards the Rwenzori Mountains in the northwest of the basin (Nicholson et al., 2000; Yin et al., 2000; Nicholson and Yin, 2002; Okonga et al., 2006), helping to explain the occurrence of surface waters in western Uganda with large d-excess values. Isotope data from the IAEA-WMO station at Entebbe, on the northern shores of the lake, confirm the occurrence of significant rainfall originating from evaporated waters of Lake Victoria (Rozanski et al., 1996).

With the above evidence in mind, we suggest that surface samples from western Uganda [1-7] and the Blue Nile [25-33] with high d-excess values represent moisture derived from recycled continental source(s), including the large water bodies found in their respective headwaters (notably Lakes Victoria and Tana), together with contributions from large swamps such as the Sudd and Bahr el Ghazal in South Sudan. It is also feasible that in addition to recycled moisture evaporated from Lake Victoria, the largest d-excess (and most isotopically depleted) values found in rivers flowing from the glacierized peaks of the Rwenzori Mountains [1-3], reflect elevated d-excess values developed during snow formation (Jouzel and Merlivat, 1984). The remainder of the River Nile surface waters have

low d-excess values (<10‰) which are consistent with evaporative losses from surface waters (Fig. 5).

5.2 DSi and $\delta^{30}Si$

The ultimate source of DSi in the major Nile sub-basins is bedrock geology (Figs. 2a and 6). Average DSi values were greatest in the Blue Nile drainage, which is predominantly underlain by trap basalts, rich in ferromagnesian minerals that are highly susceptible to chemical weathering (Cochran and Berner, 1996; Dessert et al., 2003; Dupré et al., 2003). The seasonal contrast in DSi concentrations was also greatest in the Blue Nile Basin, which has only one rainy season per year, in contrast to the bimodal but more evenly distributed rainfall regime of the White Nile headwaters. Given the steep, exposed topography of the Ethiopian Highlands, flushing of DSi from soils and desorption of Si from suspended-sediment particles can be inferred to reach a maximum during the flood season (Hall et al., 1977; Sinada and Abdel Karim, 1984). In contrast, DSi concentrations in the White Nile headwaters were lower and declined much more rapidly downstream, which can be explained by a combination of: 1) quartz-rich, granitoid bedrocks that are more resistant to weathering; and 2) rapid silica uptake by Si-accumulating plants in the densely vegetated equatorial catchments, and by diatom blooms and stands of aquatic macrophytes in the chain of large lakes and swamps (Talling, 1963, 1966; McCarthy et al., 1989). Fig. 6 shows that the Ethiopian Highlands are the predominant source of DSi for the Main Nile, along which DSi concentrations decline exponentially with latitude, due to the lack of major tributary inputs after the River Atbara.

All our water samples from the River Nile were enriched in ^{30}Si relative to expected values for local bedrock, perhaps indicating that the light isotope ^{28}Si had been preferentially removed through formation of pedogenic minerals, phytoliths or diatom frustules. Based on our current dataset alone, we cannot rule out fractionation of Si isotopes by neoformation of amorphous silica and clays as an important process in the Si cycle in the Nile Basin (Basile-Doelsch, 2006; Opfergelt et al. 2008). However, the large range of $\delta^{30}Si$ values in surface waters and their progressive downstream enrichment (Fig. 7) are consistent with intense Si cycling by aquatic ecosystems (Ding et al. 2004; Engström et al. 2010; Ding et al. 2011). Seasonal contrasts observed in both DSi concentrations and $\delta^{30}Si$ values are most readily explained by strong coupling between DSi supply and biological demand. In general, DSi concentrations were lowest during the dry season, when soil moisture and runoff in the catchments were reduced, inhibiting the mobilisation of Si from soils and sediments, and reducing the availability of DSi for biological uptake. The reduction in DSi concentrations

during the dry season corresponded to a rise in $\delta^{30}Si$ values (Fig. 8), indicating that biological demand for DSi exceeded supply. This was particularly apparent in the headwater lakes, and will be discussed in detail later. In contrast, wet-season DSi concentrations were higher and the corresponding $\delta^{30}Si$ values were lighter. This suggests that increased mobilization of Si from the catchments occurred during the rains, when an influx of turbid floodwaters would also tend to inhibit diatom productivity (Talling et al., 2009), thereby decreasing biological uptake of the light isotope ^{28}Si compared with the dry season. Engström et al. (2010) observed similar isotope variations in DSi in a river in northern Sweden, where a combination of seasonal discharge from snowmelt, vegetation changes and lacustrine diatom productivity significantly affected the DSi transport in the basin.

The lowest DSi concentrations were found in the headwater lakes or their outflows (e.g. Lakes Victoria, Albert and Tana) and in the lower reaches of the Nile [45-47], in association with elevated $\delta^{30}Si$ values (Figs. 6 and 8). Once again, this inverse relationship (low DSi, high $\delta^{30}Si$) can be attributed to the balance between DSi supply and demand. Immediately surrounding the headwater lakes are extensive wetland areas containing known Si-accumulator plants such as *Cyperus papyrus*, *Phragmites* and other emergent macrophytes that are likely to take up significant amounts of Si (Gaudet, 1977; McCarthy et al., 1989; Hodson et al., 2005; Struyf et al., 2007; Struyf and Conley, 2009; Schoelynck et al., 2010). Si extraction by accumulator plants and diatom blooms during the dry season would significantly reduce the amount of DSi in the lake waters, driving up $\delta^{30}Si$ values. In the lower reaches of the Nile, low DSi concentrations and strongly enriched $\delta^{30}Si$ values also reflect an excess of demand over supply. The Main Nile lacks major tributary inputs for the last ~2700 km of its course through the Eastern Sahara. Terrestrial vegetation is greatly reduced by the hyperarid climate, which also limits the supply of DSi resulting from silicate-rock weathering by plants along this stretch, causing in a rapidly diminishing stock as Si is taken up by Si-accumulating organisms such as diatoms. Storage of floodwaters in reservoirs behind large dams sited along the Main Nile (e.g. Jebel Aulia, Merowe and Aswan) had a similar effect to that of the headwater lakes, since they hold back the flux of Si downstream and enhance uptake of DSi by aquatic organisms (Humborg et al., 2000).

Several anomalous sites in the White Nile headwaters [3 & 4, 7] displayed very light $\delta^{30}Si$ values, although still greatly enriched relative to the expected $\delta^{30}Si$ signature of the local bedrock (–0.10 to –0.07‰: André et al. (2006)) (Fig. 8). These rivers drain the Rwenzori and Virunga Mountains, respectively. It is suggested that bare rock surfaces, thin soils and sparse vegetation cover on the upper slopes of these mountains retard chemical weathering

(Moulton et al., 2000) and Si biocycling (Georg et al., 2006a), resulting in a combination of low DSi concentrations and depleted $\delta^{30}Si$ values.

Si biocycling appears to be most intense in the Blue Nile Basin, particularly during the dry season, as the difference between the expected $\delta^{30}Si$ composition of the local rock (basalt: –0.29‰ ± 0.08‰ (Savage et al., 2011)) and the river waters is greater than in the White Nile Basin (Fig. 6). Several factors may account for this large fractionation. Sampling was undertaken at the end of the dry season, immediately before the rains began, when it is likely that the supply of DSi was at its lowest whilst biological demand was at its peak. The $\delta^{30}Si$ value of the outflow from Lake Tana [35] was already significantly enriched relative to the expected range of values for basalt and to the Blue Nile further downstream [34], indicating that a large proportion of this enrichment occurred in the headwaters. It seems likely that towards the end of the dry season, availability of DSi within the Tana catchment was very limited, causing the $\delta^{30}Si$ values of river waters to rise as biological demand persisted.

Although the positive correlation observed between $\delta^{18}O$ and $\delta^{30}Si$ during the wet season (Fig. 9) is not directly causal, both isotope ratios evolved in parallel due to cumulative downstream losses of the light isotopes ^{16}O through evaporation and ^{28}Si through biological uptake. In contrast, during the dry season, anthropogenic impacts on the hydrological cycle and intense local biocycling of Si obscured any general trend. When outliers clearly affected by water-management practices (i.e. irrigation and major reservoirs) were removed [sites: 25, 13 & 41 during the dry season], a similar positive trend to the wet season was observed, although with higher values of both $\delta^{30}Si$ and $\delta^{18}O$ (updated regression not shown: R^2 = 0.023, p = 0.622). However, the trendline is still not significant after the removal of these three outliers, it is likely that the isotope values of other samples from the Main Nile were affected by human activity to a less obvious degree. Based on the wet-season dataset alone, Si supply from the Nile headwaters (represented by $\delta^{30}Si$) appears to be strongly linked to catchment hydrology (represented by $\delta^{18}O$), which is not surprising given that mobilisation of DSi from soils and sediments is primarily dependent on rainfall and runoff.

5.3 Implications for interpreting the Quaternary palaeorecord

During the Middle to Late Quaternary, tropical Africa was strongly affected by quasi-periodic variations in the Earth's orbital parameters. During boreal-summer insolation maxima, monsoon rains penetrated deep into the Sahara, causing a northward migration of the major vegetation belts, increases in river discharge, and an expansion of lakes and wetlands

(Kutzbach and Street-Perrott, 1985; Kutzbach and Liu, 1997). Changes to the hydrology and in terrestrial and aquatic ecosystems in the Nile Basin during this period are becoming increasingly well documented from the sediment record (dune sands, river deposits, lake sediments, and Mediterranean sapropels) (Williams et al., 2006; Williams et al., 2010). At the Last Glacial Maximum (LGM, ~21ka), tropical Africa was generally drier and colder, resulting in desiccation of several of the headwater lakes (Victoria, Albert and Tana) and their isolation from the Nile (Johnson et al., 1996; Talbot and Lærdal, 2000; Beuning et al., 1997; Lamb et al., 2007; Stager and Johnson, 2008). White Nile discharge was low and extremely seasonal, while the Blue Nile flood was even more flashy than today (Adamson et al., 1980; Williams et al., 2000). Refilling and overflow of the White Nile headwater lakes and Lake Tana began around 14.5 ka BP, marking the abrupt onset of the enhanced summer monsoon and the so-called "Wild Nile" (Talbot et al., 2000; Williams et al., 2006; Lamb et al., 2007). During the interval ~15 ka to 5 ka BP, a general increase in rainfall across the entire Nile Basin, apart from the northernmost Sahara, resulted in enhanced vegetation cover and river discharge; perennial flow into the Nile from large Saharan wadi systems (Pachur and Kröpelin, 1987); and widespread proliferation of lakes and swamps. A 450 km^2 palaeolake west of the Main Nile in northern Sudan (Williams et al., 2010) and a greatly enlarged Lake Qarun near Cairo (≤ 2100 km^3: Hassan (1986)) were fed by increased overspill of Nile floodwaters. From mid-Holocene to present, the climate of the Nile Basin has become much drier due to the retreat of the enhanced monsoon, and the modern discharge regime of the Nile has been established.

Our modern seasonal isotope data suggest that changes in rainfall induced by orbital forcing would have had synergistic impacts on the water and Si cycles in the Nile Basin. Wetter and more humid conditions during the early- to mid-Holocene were associated with a decrease in evaporative enrichment of surface waters, recorded by lower $\delta^{18}O$ values in aquatic cellulose and subfossil mollusca (Abell and Hoelzmann, 2000; Beuning et al., 2002). With increased moisture availability and shorter dry seasons, terrestrial plant productivity would have increased, promoting silicate weathering. Increased runoff volumes and more perennial flow from a larger and more integrated drainage network (Talbot et al., 2000), would have generated an excess influx of DSi into the Nile, probably reducing $\delta^{30}Si$ values in surface waters despite the concurrent increase in the total area of swamps and open water. In contrast, during the LGM and the late Holocene, which were characterized by expansion of arid and semiarid environments enhanced evaporation resulting from lower humidity would have enriched the heavy isotopes ^{2}H and ^{18}O in surface waters. The influx of DSi from the shrunken and more seasonal drainage network would have declined, driving up the $\delta^{30}Si$ values of lake and river waters. In summary, under different climate regimes, the delivery of

DSi from the River Nile to the Mediterranean Sea would have been modified. During drier periods, the DSi flux from the Nile Delta may have diminished as a result of decreased weathering and DSi input to the river system relative to biological demand, causing a significant reduction in the supply of Si for marine diatoms, which dominate CO_2 drawdown by the oceanic biological pump (Smetacek, 1998; Yool and Tyrrell, 2003).

6 Conclusions

Stable isotopes of H, O and Si in surface waters from the Nile Basin were used as tracers for the hydrological and Si cycles, respectively. Large seasonal shifts in H- and O-isotope compositions reflected changes in water balance. During the dry season, lower humidity favoured evaporative enrichment of surface waters and cumulative downstream losses from swamps and open water bodies. The Main Nile showed the greatest evaporative enrichment, due to the year-round arid climate and lack of rainfall or tributary input for 2700 km downstream from its confluence with the Atbara. Seasonal changes in DSi concentrations and Si isotopes provide useful information on Si cycling under different climate regimes in the Nile Basin. This study has increased the global upper limit of δ^{30}Si for dissolved Si in natural waters by more than 1‰. Contrasting geology in the headwaters of the White and Blue Nile is clearly reflected in DSi concentrations, with the highest levels in the Blue Nile headwaters due to the basaltic bedrock and steep, easily erodible, sparsely vegetated slopes of the Ethiopian Highlands. Low DSi concentrations and correspondingly enriched Si-isotope values are found in the headwater lakes and in the Main Nile where depletion of Si by aquatic organisms (notably diatoms and macrophytes) is thought to be important. Extensive downstream enrichment of Si isotopes and depletion of DSi during both wet and dry seasons in the River Nile imply active Si biocycling. The heavy isotope ^{30}Si is enriched in surface waters during the dry season due to a reduction in mobilisation of DSi from the catchment relative to aquatic demand. Localized anthropogenic impacts on the isotope composition of surface waters are identifiable with respect to both the hydrological and Si cycles, especially during the dry season and along the Main Nile where irrigation and retention of stored floodwaters behind large dams are most prevalent.

Modern seasonal variations of DSi and δ^{30}Si in the River Nile indicate that the Si flux from large tropical rivers to the oceans is not constant and is likely to be highly variable on Quaternary time scales. In future, coupled measurements of the O- and Si-isotope compositions of freshwater diatom frustules preserved in sediment records have the potential to clarify the relationship between water balance and Si cycling in different geological and climatic settings. On a glacial / interglacial time scale, variations in the

riverine Si flux from the continents may have had a significant impact on the marine Si budget and consequently on the global C cycle.

7 Acknowledgements

This research was funded by a NERC Doctoral Training Grant (NE/G524352/1) awarded to Helen Cockerton and a National Geographic Society Grant for Research and Exploration (8829-10). Isotopic analyses were carried out at the NERC Isotope Geosciences Laboratory, UK under award IP-1151-1109. The authors would like to thank Carol Arrowsmith (NIGL) for the stable H- and O-isotope analysis and Simon Chenery and Thomas Barlow (BGS) for the ICP-MS analysis of the dissolved silicon concentrations. Research was conducted with permission of the Ugandan National Council of Science and Technology (No. NS 319) and the Uganda Wildlife Authority (UWA/FOD/33/02). The authors are grateful for the field assistance provided by Charlotte Bristol, Alexandra Goldsack, Morgan Andama, Sarah Cockerton and Mark Fox. We thank Nicola Jones Anna Ratcliffe for helping prepare the figures.

8 References

Abell, P.I., Hoelzmann, P., 2000. Holocene palaeoclimates in northwestern Sudan: stable isotope studies on molluscs. Global and Planetary Change 26, 1-12.

Abu-Zied, M.A., El-Shibini, F.Z., 1997. Egypt's High Aswan Dam. Water Resources Development 13, 209-217.

Adamson, D.A., Gasse, F., Street, F.A., Williams, M.A.J., 1980. Late Quaternary history of the Nile. Nature 288, 50-55.

Alexandre, A., Bouvet, M., Abbadie, L., 2011. The role of savannas in the terrestrial Si cycle: a case-study from Lamto, Ivory Coast. Global and Planetary Change 78, 162-169.

Alexandre, A., Meunier, J.D., Colin, F., Koud, J.M., 1997. Plant impact on the biogeochemical cycle of silicon and related weathering processes. Geochimica et Cosmochimica Acta 61, 677-682.

Alleman, L.Y., Cardinal, D., Cocquyt, C., Plisnier, P.-D., Descy, J.-P., Kimirei, I., Sinyinza, D., André, L., 2005. Silicon isotopic fractionation in Lake Tanganyika and its main tributaries. Journal of Great Lakes Research 31, 509-519.

André, L., Cardinal, D., Alleman, L.Y., Moorbath, S., 2006. Silicon isotopes in ~3.8 Ga West Greenland rocks as a clue to the Eoarchaean supracrustal Si cycle. Earth and Planetary Science Letters 245, 162-173.

Araguás-Araguás, L., Fröhlich, K., Rozanski, K., 2000. Deuterium and oxygen-18 isotope composition of precipitation and atmospheric moisture. Hydrological Processes 14, 1341-1355.

Bartoli, F., 1983. The biogeochemical cycle of silicon in two temperate forest ecosystems. Ecological Bulletin 35, 469-476.

Basile-Doelsch, I., 2006. Si stable isotopes in the Earth's surface: a review. Journal of Geochemical Exploration 88, 252-256.

Berner, R.A., 1994. GEOCARB II: a revised model of atmospheric CO_2 over Phanerozoic time. American Journal of Science 294, 56-91.

Berner, R.A., 1995. Chemical weathering and its effect on atmospheric CO_2 and climate. Reviews in Mineralogy 31, 565-583.

Berner, R.A., Lasaga, A.C., Garrels, R.M., 1983. The carbonate-silicate geochemical cycle and its effect on atmospheric carbon dioxide over the past 100 million years. American Journal of Science 283, 641-683.

Beuning, K.R.M., Kelts, K., Russell, J., Wolfe, B.B., 2002. Reassessment of Lake Victoria-Upper Nile River paleohydrology from oxygen isotope records of lake-sediment cellulose. Geology 30, 559-562.

Beuning, K.R.M., Talbot, M.R., Kelts, K., 1997. A revised 30,000-year paleoclimatic and paleohydrologic history of Lake Albert, East Africa. Palaeogeography, Palaeoclimatology, Palaeoecology 136, 259-279.

Blecker, S.W., McCulley, R.L., Chadwick, O.A., Kelly, E.F., 2006. Biologic cycling of silica across a grassland bioclimosequence. Global Biogeochemical Cycles 20, GB3023.

Brady, P.V., Carroll, S.A., 1994. Direct effects of CO_2 and temperature on silicate weathering: possible implications for climate control. Geochimica et Cosmochimica Acta 58, 1853-1856.

Camberlin, P., 2009. Nile basin climates, In: Dumont, H.J. (Ed.), The Nile: origin, environments, limnology and human use. Springer-Verlag, New York, pp. 307-333.

Cardinal, D., Alleman, L.Y., de Jong, J., Ziegler, K., André, L., 2003. Isotopic composition of silicon measured by multicollector plasma source mass spectrometry in dry plasma mode. Journal of Analytical Atomic Spectrometry 18, 213-218.

Cardinal, D., Gaillardet, J., Hughes, H.J., Opfergelt, S., André, L., 2010. Contrasting silicon isotope signatures in rivers from the Congo Basin and the specific behaviour of organic-rich waters. Geophysical Research Letters 37, L12403.

Clark, I.D., Fritz, P., 1997. Environmental isotopes in hydrogeology. CRC Press, Florida.

Cochran, M.F., Berner, R.A., 1996. Promotion of chemical weathering by higher plants: field observations on Hawaiian basalts. Chemical Geology 132, 71-77.

Cohen, A.S., Talbot, M.R., Awramik, S.M., Dettman, D.L., Abell, P., 1997. Lake level and palaeoenvironmental history of Lake Tanganyika, Africa, as inferred from late Holocene and modern stromatolites. Geological Society of America Bulletin 109, 444-460.

Conley, D.J., 1997. Riverine contribution of biogenic silica to the oceanic silica budget. Limnology and Oceanography 42, 774-777.

Conley, D.J., 2002. Terrestrial ecosystems and the global biogeochemical silica cycle. Global Biogeochemical Cycles 16, 68.61-68.68.

Conway, D., 1997. A water balance model of the Upper Blue Nile in Ethiopia. Hydrological Sciences-Journal des Sciences Hydrologiques 42, 265-286.

Conway, D., 2000. The climate and hydrology of the upper Blue Nile River. The Geographical Journal 166, 49-62.

Craig, H., 1961. Isotopic variations in meteoric waters. Science 133, 1702-1703.

Craig, H., Gordon, L.I., 1965. Deuterium and oxygen-18 variations in the ocean and marine atmosphere, In: Tongiorgi, E. (Ed.), Stable isotopes in oceanographic studies and paleotemperatures, V. Lischi, Spoleto, Italy, pp. 9-130.

Dansgaard, W., 1964. Stable isotopes in precipitation. Tellus 16, 436-468.

De La Rocha, C.L., Brzezinski, M.A., DeNiro, M.J., 2000. A first look at the distribution of the stable isotopes of silicon in natural waters. Geochimica et Cosmochimica Acta 64, 2467-2477.

Dessert, C., Dupré, B., Gaillardet, J., François, L.M., Allègre, C.J., 2003. Basalt weathering laws and the impact of basalt weathering on the global carbon cycle. Chemical Geology 202, 257-273.

Ding, T., Wan, D., Wang, C., Zhang, F., 2004. Silicon isotope compositions of dissolved silicon and suspended matter in the Yangtze River, China. Geochimica et Cosmochimica Acta 68, 205-216.

Ding, T.P., Gao, J.F., Tian, S.H., Wang, H.B., Li, M., 2011. Silicon isotopic composition of dissolves silicon and suspended particulate matter in the Yellow River, China, with implications for the global silicon cycle. Geochimica et Cosmochimica Acta 75, 6672-6689.

Dugdale, R.C., Wilkerson, F.P., 2001. Sources and fates of silicon in the ocean: the role of diatoms in the climate and glacial cycles. Scientia Marina 65, 141-152.

Dupré, B., Dessert, C., Oliva, P., Goddéris, Y., Viers, J., François, L., Millot, R., Gaillardet, J., 2003. Rivers, chemical weathering and Earth's climate. Comptes Rendus Geoscience 335, 1141-1160.

Engström, E., Rodushkin, I., Baxter, D.C., Öhlander, B., 2006. Chromatographic Purification for the Determination of Dissolved Silicon Isotopic Compositions in Natural Waters by High-Resolution Multicollector Inductively Coupled Plasma Mass Spectrometry. Analytical Chemistry 78, 250-257.

Engström, E., Rodushkin, I., Ingri, J., Baxter, D.C., Ecke, F., Österlund, H., Öhlander, B., 2010. Temporal isotopic variations of dissolved silicon in a pristine boreal river. Chemical Geology 271, 142-152.

Epstein, E., 1999. Silicon. Annual Review of Plant Physiology and Plant Molecular Biology 50, 641-664.

Flohn, H., Fraedrich, K., 1966. Tagesperiodische zirkulation und niederschlagsverteilung am Viktoria-See (Ostafrika). Meteorologische Rundschau 19, 157-165.

Foucault, A., Stanley, D.J., 1989. Late quaternary palaeoclimatic oscillations in East Africa recorded by heavy minerals in the nile delta. Nature 339, 44-46.

Fritz, P., 1981. River waters, In: Gat, J.R., Gonfiantini, R. (Eds.), Stable Isotope Hydrology: Deuterium and Oxygen-18 in the Water Cycle. IAEA Technical Report Series 210, pp. 177-201.

Fröhlich, K., Gibson, J.J., Aggarwal, P.K., 2002. Deuterium excess in precipitation and its climatological significance, Study of Environmental Change using Isotope Techniques. International Atomic Energy Agency, International Conference in Vienna, Austria, 23–27 April 2001, pp. 54-65.

Furon, R., 1958. Esquisse structurale Provisoire de l'Afrique, 1 : 10,000,000. Association des Services Geologiques Africains (ASGA) Congrès Géologique International.

Gaillardet, J., Dupré, B., Louvat, P., Allègre, C.J., 1999. Global silicate weathering and CO_2 consumption rates deduced from the chemistry of large rivers. Chemical Geology 159, 3-30.

Gat, J.R., 1996. Oxygen and hydrogen isotopes in the hydrological cycle. Annual Review of Earth and Planetary Science 24, 225-262.

Gat, J.R., 2000. Atmospheric water balance-the isotopic perspective. Hydrological Processes 14, 1357-1369.

Gat, J.R., Bowser, C.J., Kendall, C., 1994. The contribution of evaporation from the Great Lakes to the continental atmosphere: estimate based on stable isotope data. Geophysical Research Letters 21, 557-560.

Gat, J.R., Matsui, E., 1991. Atmospheric water balance in the Amazon Basin: an isotopic evapotranspiration model. Journal of Geophysical Research 96, 13,179-113,188.

Gaudet, J.J., 1977. Uptake, accumulation, and loss of nutrients by papyrus in tropical swamps. Ecology 58, 415-422.

Georg, R.B., Reynolds, B.C., Frank, M., Halliday, A.N., 2006a. Mechanisms controlling the silicon isotopic compositions of river waters. Earth and Planetary Science Letters 249, 290-306.

Georg, R.B., Reynolds, B.C., Frank, M., Halliday, A.N., 2006b. New sample preparation techniques for the determination of Si isotopic compositions using MC-ICPMS. Chemical Geology 235, 95-104.

Georg, R.B., Reynolds, B.C., West, A.J., Burton, K.W., Halliday, A.N., 2007. Silicon isotope variations accompanying basalt weathering in Iceland. Earth and Planetary Science Letters 261, 476–490.

Georg, R.B., West, A.J., Basu, A.R., Halliday, A.N., 2009. Silicon fluxes and isotope composition of direct groundwater discharge into the Bay of Bengal and the effect on the global ocean silicon isotope budget. Earth and Planetary Science Letters 283, 67–74.

Gonfiantini, R., Roche, M.-A., Olivry, J.-C., Fontes, J.-C., Zuppi, G.M., 2001. The altitude effect on the isotopic composition of tropical rains. Chemical Geology 181, 147-167.

Green, J., 2009. Nilotic Lakes of the Western Rift, In: Dumont, H.J. (Ed.), The Nile: origin, environments, limnology and human use. Springer Science + Business Media B.V., pp. 263-286.

Green, J., El-Moghraby, A.I., 2009. Swamps of the upper White Nile, In: Dumont, H.J. (Ed.), The Nile: origin, environments, limnology and human use. Springer Science + Business Media B.V., pp. 193-204.

Hall, A., Valente, I.M.C.B.S., Davies, B.R., 1977. The Zambezi river in Moçambique: the physico- chemical status of the middle and lower Zambezi prior to the closure of the Cabora Bassa Dam. Freshwater Biology 7, 187-206.

Harrison, K.G., 2000. Role of increased marine silica input on paleo-pCO_2 levels. Paleoceanography 15, 292-298.

Hassan, F., 1986. Holocene lakes and prehsitoric settlements of the Western Faiyum, Egypt. Journal of Archaeological Science 13, 483-501.

Hilley, G., Porder, S., 2008. A framework for predicting global silicate weathering and CO_2 drawdown rates over geologic time-scales. Proceedings of the National Academy of Sciences of the United States of America 105, 16855-16859.

Hinsinger, P., Barros, O.N.F., Benedetti, M.F., Noack, Y., Callot, G., 2001. Plant-induced weathering of a basaltic rock: experimental evidence. Geochimica et Cosmochimica Acta 65, 137-152.

Hodson, M.J., White, P.J., Mead, A., Broadley, M.R., 2005. Phylogenetic variation in the silicon composition of plants. Annals of Botany 96, 1027-1046.

Hughes, H.J., Bouillon, S., André, L., Cardinal, D., 2012. The effects of weathering variability and anthropogenic pressures upon silicon cycling in an intertropical watershed (Tana River, Kenya). Chemical Geology 308-309, 18-25.

Humborg, C., Conley, D.J., Rahm, L., Wulff, F., Cociasu, A., Ittekkot, V., 2000. Silicon retention in river basins: far-reaching effects on biogeochemistry and aquatic food webs in coastal marine environments. Ambio 29, 25-50.

Hurst, H.E., 1952. The Nile: a general account of the river and utilization of its waters. Constable, London.

Johnson, T.C., Scholz, C.A., Talbot, M., Kelts, K., Ricketts, R.D., Ngobi, G., Beuning, K., Ssemmanda, I., McGill, J.W., 1996. Late Pleistocene Desiccation of Lake Victoria and Rapid Evolution of Cichlid Fishes. Science 273, 1091-1093.

Jones, L.H.P., Handreck, K.A., 1967. Silica in soils, plants and animals. Advances in Agronomy 19, 107-149.

Jouzel, J., Merlivat, L., 1984. Deuterium and oxygen 18 in precipitation: modeling of the isotopic effects during snow formation. Journal of Geophysical Research 89, 11749-11757.

Kebede, S., Travi, Y., 2012. Origin of the $\delta^{18}O$ and $\delta^{2}H$ composition of meteoric waters in Ethiopia. Quaternary International 257, 4-12.

Kebede, S., Travi, Y., Alemayehu, T., Ayenew, T., 2005. Groundwater recharge, circulation and geochemical evolution in the source region of the Blue Nile River, Ethiopia. Applied Geochemistry 20, 1658-1676.

Kelly, E.F., Chadwick, O.A., Hilinski, T.E., 1998. The effect of plants on mineral weathering. Biogeochemistry 42, 21-53.

Kendall, C., Coplen, T.B., 2001. Distribution of oxygen-18 and deuterium in river waters across the United States. Hydrological Processes 15, 1363–1393.

Kendall, R.L., 1969. An ecological history of the Lake Victoria basin. Ecological Monographs 39, 121-176.

Kutzbach, J.E., Liu, Z., 1997. Response of the African monsoon to orbital forcing and ocean feedbacks in the middle Holocene. Science 278, 440-443.

Kutzbach, J.E., Street-Perrott, F.A., 1985. Milankovitch forcing of fluctuations in the level of tropical lakes from 18 to 0 kyr BP. Nature 317, 130-134.

Lamb, H.F., Bates, C.R., Coombes, P.V., Marshall, M.H., Umer, M., Davies, S.J., Dejen, E., 2007. Late Pleistocene desiccation of Lake Tana, source of the Blue Nile. Quaternary Science Reviews 26, 287-299.

Langdale-Brown, I., Osmaston, H.A., J.G., W., 1964. The vegetation of Uganda and its bearing on land use. Government of Uganda, Entebbe.

Leng, M.J., Barker, P.A., 2006. A review of the oxygen isotope composition of lacustrine diatom silica for palaeoclimate reconstruction. Earth Science Reviews 75, 5-27.

Leng, M.J., Marshall, J.D., 2004. Palaeoclimate interpretation of stable isotope data from lake sediment archives. Quaternary Science Reviews 23, 811-831.

Leng, M.J., Swann, G.E.A., 2010. Stable isotopes in diatom silica, In: Smol, J.P., Stoermer, E.F. (Eds.), The diatoms : applications for the environmental and earth sciences. Cambridge University Press, Cambridge, UK, pp. 127-143.

Leng, M.J., Swann, G.E.A., Hodson, M.J., Tyler, J.J., Patwardhan, S.V., Sloane, H.J., 2009. The potential use of silicon isotope composition of biogenic silica as a proxy for environmental change. Silicon 1, 65-77.

Levin, N.E., Zipser, E.J., Cerling, T.E., 2009. Isotopic composition of waters from Ethiopia and Kenya: Insights into moisture sources for eastern Africa. Journal of Geophysical Research 114, D23306.

Lucas, Y., 2001. The role of plants in controlling rates and products of weathering: importance of biological pumping. Annual Review of Earth and Planetary Sciences 29, 135-163.

Ma, J.F., Miyake, Y., Takahashi, E., 2001. Silicon as a beneficial element for crop plants, In: Datnoff, L.E., Snyder, G.H., Korndörfer, G.H. (Eds.), Silicon in Agriculture. Elsevier, Amsterdam, pp. 17-39.

McCarthy, T.S., McIver, J.R., Cairncross, B., Ellery, W.N., Ellery, K., 1989. The inorganic geochemistry of peat from the Maunachira channel swamp system, Okavango Delta, Botswana. Geochimica et Cosmochimica Acta 53, 1077-1089.

Merlivat, L., Jouzel, J., 1979. Global climatic interpretation of the deuterium-oxygen 18 relationship for precipitation. Journal of Geophysical Research 84, 5029-5033.

Mohamed, Y.A., van den Hurk, B.J.J.M., Savenije, H.H.G., Bastiaanssen, W.G.M., 2005. Impact of the Sudd wetland on the Nile hydroclimatology. Water Resources Research 41, W08420.

Moulton, K.L., West, J., Berner, R.A., 2000. Solute flux and mineral mass balance approaches to the quantification of plant effects on silicate weathering. American Journal of Science 300, 539-570.

Nicholson, S.E., 1996. A review of climate dynamics and climate variability in Eastern Africa, In: Johnson, T.C., Odada, E.O. (Eds.), The Limnology, Climatology and Paleoclimatology of the East African Lakes. Gordon and Breach Publishers, Amsterdam, The Netherlands, pp. 25-56.

Nicholson, S.E., 2009. A revised picture of the structure of the "monsoon" and land ITCZ over West Africa. Climate Dynamics 32, 1155-1171.

Nicholson, S.E., Yin, X., 2002. Mesoscale patterns of rainfall, cloudiness and evaporation over the Great Lakes of East Africa, In: Odada, E.O., Olago, D.O. (Eds.), The East African Great Lakes: Limnology, Palaeolimnology and Biodiversity. Kluwer, Dordrecht, pp. 93–119.

Nicholson, S.E., Yin, X., Ba, M.B., 2000. On the feasibility of using a lake water balance model to infer rainfall: an example from Lake Victoria. Hydrological Sciences-Journal des Sciences Hydrologiques 45, 75-95.

Nyssen, J., Vandenreyken, H., Poesen, J., Moeyersons, J., Deckers, J., Haile, M., Salles, C., Govers, G., 2005. Rainfall erosivity and variability in the Northern Ethiopian Highlands. Journal of Hydrology 311, 172-187.

Okonga, J.R., Sewagudde, S.M., Mngodo, R.J., Sangale, F.D., Mwanuzi, F.L., Hecky, R.E., 2006. Water balance of Lake Victoria, In: Odada, E.O., Olago, D.O. (Eds.), Proceedings of the 11th World Lakes Conference, Nairobi, Kenya, pp. 47-56.

Opfergelt, S., Delvaux, B., André, L., Cardinal, D., 2008. Plant silicon isotopic signature might reflect soil weathering degree. Biogeochemistry 91, 163-175.

Opfergelt, S., Eiriksdottir, E.S., Burton, K.W., Einarsson, A., Siebert, C., Gislason, S.R., Halliday, A.N., 2011. Quantifying the impact of freshwater diatom productivity on silicon isotopes and silicon fluxes: Lake Myvatn, Iceland. Earth and Planetary Science Letters 305, 73–82.

Pachur, H.-J., Kröpelin, S., 1987. Wadi Howar: paleoclimatic evidence from an extinct river system in the southeastern Sahara. Science 237, 298-300.

Ragueneau, O., Schultes, S., Bidle, K., Claquin, P., Moriceau, B., 2006. Si and C interactions in the world ocean: Importance of ecological processes and implications for the role of diatoms in the biological pump. Global Biogeochemical Cycles 20, GB4S02.

Raven, J.A., 1983. The transport and function of silicon in plants. Biological Reviews 58, 179-207.

Reynolds, B.C., Aggarwal, J., Andre, L., Baxter, D., Beucher, C., Brzezinski, M.A., Engstrom, E., Georg, R.B., Land, M., Leng, M.J., Opfergelt, S., Rodushkin, I., Sloane, H.J., van den Boorn, S.H.J.M., Vroon, P.Z., Cardinal, D., 2007. An inter-laboratory comparison of Si isotope reference materials. Journal of Analytical Atomic Spectrometry 22, 561-568.

Round, F.E., Crawford, R.M., Mann, D.G., 1990. The Diatoms: biology and morphology of the genera. Cambridge University Press, Cambridge, UK.

Rozanski, K., Araguas-Araguas, L., Gonfiantini, R., 1996. Isotope patterns of precipitation in the East African region, In: Johnson, T.C., Odada, E.O. (Eds.), The Limnology, Climatology

and Paleoclimatology of the East African Lakes. Gordon and Breach Publishers, Amsterdam, The Netherlands, pp. 79-93.

Salati, E., A., D.O., Matsui, E., Gat, J.R., 1979. Recycling of water in the Amazon Basin: an isotopic study. Water Resources Research 15, 1250-1258.

Savage, P.S., Georg, R.B., Williams, H.M., Burton, K.W., Halliday, A.N., 2011. Silicon isotope fractionation during magmatic differentiation. Geochimica et Cosmochimica Acta 75, 6124-6139.

Schlüter, T., 2008. Geological atlas of Africa: With Notes on Stratigraphy, Tectonics, Economic Geology, Geohazards, Geosites and Geoscientific Education of Each Country, 2nd ed. Springer-Verlag, Berlin.

Schoelynck, J., Bal, K., Backx, H., Okruszko, T., Meire, P., Struyf, E., 2010. Silica uptake in aquatic and wetland macrophytes: a strategic choice between silica, lignin and cellulose? New Phytologist 186, 385-391.

Shahin, M., 1985. Hydrology of the Nile Basin. Elsevier, Amsterdam.

Sinada, F., Abdel Karim, A.G., 1984. Physical and chemcial characteristics of the Blue Nile and the White Nile at Khartoum. Hydrobiologia 110, 21-32.

Smetacek, V., 1998. Diatoms and the silicate factor. Nature 391, 224-225.

Sonntag, E., Klitzsch, E., Lohnert, E.P., El-Shazly, E.M., Munnich, K.O., Junghans, C., Thorweihe, U., Weistroffer, K., Swailem, F.M., 1979. Palaeoclimatic information from deuterium and oxygen-18 in carbon-14 dated north Saharian groundwaters, Isotope Hydrology 1978, vol. II. International Atomic Energy Agency, Vienna.

Stager, J.C., Johnson, T.C., 2008. The late Pleistocene desiccation of Lake Victoria and the origin of its endemic biota Hydrobiologia 596, 5-16.

Stewart, M.K., 1975. Stable Isotope Fractionation Due to Evaporation and Isotopic Exchange of Falling Waterdrops: Applications to Atmospheric Processes and Evaporation of Lakes. Journal of Geophysical Research 80, 1133-1146.

Street-Perrott, F.A., Barker, P.A., 2008. Biogenic silica: a neglected component of the coupled global continental biogeochemical cycles of carbon and silicon. Earth Surface Processes and Landforms 33, 1436-1457.

Street-Perrott, F.A., Barker, P.A., Leng, M., J., Sloane, H.J., Wooller, M.J., Ficken, K.J., Swain, D.L., 2008. Towards an understanding of late Quaternary variations in the continental biogeochemical cycle of silicon: multi-isotope and sediment-flux data for Lake Rutundu, Mt Kenya, East Africa, since 38 ka BP. Journal of Quaternary Science 23, 375-387.

Struyf, E., Conley, D.J., 2009. Silica: an essential nutrient in wetland biogeochemistry. Frontiers in Ecology and the Environment 7, 88-94.

Struyf, E., Damme, S.V., Gribsholt, B., Meire, P., 2005. Freshwater marshes as dissolved silica recyclers in an estuarine environment (Schelde estuary, Belgium). Hydrobiologia 540, 69-77.

Struyf, E., Smis, A., Van Damme, S., Meire, P., Conley, D.J., 2009. The global biogeochemical silicon cycle. Silicon 1, 207-213.

Struyf, E., Van Damme, S., Gribsholt, B., Bal, K., Beauchard, O., Middelburg, J., Meire, P., 2007. Phragmites australis and silica cycling in tidal wetlands. Aquatic botany 87, 134-140.

Sutcliffe, J.V., 1974. A hydrological study of the southern Sudd region of the Upper Nile. Hydrological Sciences Bulletin 19, 237-255.

Sutcliffe, J.V., Parks, Y.P., 1999. The Hydrology of the Nile, IAHS Special Publications. International Association of Hydrological Sciences Press, Wallingford, UK.

Talbot, M.R., Lærdal, T., 2000. The Late Pleistocene - Holocene palaeolimnology of Lake Victoria, East Africa, based upon elemental and isotopic analyses of sedimentary organic matter. Journal of Paleolimnology 23, 141-164.

Talbot, M.R., Williams, M.A.J., Adamson, D.A., 2000. Strontium isotope evidence for late Pleistocene reestablishment of an integrated Nile drainage network. Geology 28, 343-346.

Talling, J.F., 1963. Origin of stratification in an African Rift lake. Limnology and Oceanography 8, 68–78.

Talling, J.F., 1966. The annual cycle of stratification and phytoplankton growth in Lake Victoria (East Africa). Internationale Revue der gesamten Hydrobiologie 51, 545–621.

Talling, J.F., Sinada, F., Taha, O.E., Sobhy, E.M.H., 2009. Phytoplankton: composition, development and productivity, In: Dumont, H.J. (Ed.), The Nile: origins, environmens, limnology and human use. Springer Science + Business Media B.V., pp. 431-462.

Tréguer, P., Pondaven, P., 2000. Silica control of carbon dioxide. Nature 406, 358-359.

van den Boorn, S.H.J.M., Vroon, P.Z., van Belle, C.C., van der Wagt, B., Schwieters, J., van Bergen, M.J., 2006. Determination of silicon isotope ratios in silicate materials by high-resolution MC-ICP-MS using a sodium hydroxide sample digestion method. Journal of Analytical Atomic Spectrometry 21, 734-742.

White, A.F., Blum, A.E., 1995. Effects of climate on chemical weathering in watersheds. Geochimica et Cosmochimica Acta 59, 1729-1747.

White, F., 1983. The vegetation of Africa. A descriptive memoir to accompany the UNESCO/AETFAT/UNSO vegetation map of Africa. UNESCO, Paris.

Williams, M., Talbot, M., Aharon, P., Salaam, Y.A., Williams, F., Brendeland, K.I., 2006. Abrupt return of the summer monsoon 15,000 years ago: new supporting evidence from the lower White Nile valley and Lake Albert. Quaternary Science Reviews 25, 2651-2665.

Williams, M.A.J., Adamson, D., Cock, B., McEvedy, R., 2000. Late Quaternary environments in the White Nile region, Sudan. Global and Planetary Change 26, 305-316.

Williams, M.A.J., Williams, F.M., Duller, G.A.T., Munro, R.N., El Tom, O.A.M., Barrows, T.T., Macklin, M., Woodward, J., Talbot, M.R., Haberlah, D., Fluin, J., 2010. Late Quaternary floods and droughts in the Nile valley, Sudan: new evidence from optically stimulated luminescence and AMS radiocarbon dating. Quaternary Sciences Reviews 29, 1116-1137.

World Bank, 2008. Project appraisal document on a proposed credit in the amount of SDR 27.4 million (US$45 million equivalent) to the federal Democratic Republic of Ethiopia for a Tana and Beles integrated water resources development project. World Bank, Washington DC, USA.

Yin, X., Nicholson, S.E., Ba, M.B., 2000. On the diurnal cycle of cloudiness over Lake Victoria and its influence on evaporation from the lake. Hydrological Sciences-Journal des Sciences Hydrologiques 45, 407-424.

Yool, A., Tyrrell, T., 2003. Role of diatoms in regulating the ocean's silicon cycle. Global Biogeochemical Cycles 17, 1103.

Young, E.D., Galy, A., Nagahara, H., 2002. Kinetic and equilibrium mass-dependent isotope fractionation laws in nature and their geochemical and cosmochemical significance. Geochimica et Cosmochimica Acta 66, 1095-1104.

Table 1

Sample site locations and their corresponding isotopic (H, O and Si) and compositional data.

			Wet season												
Site No.		Sample site name and location	Date (month-year)	Latitude (decimal degrees)	Longitude (decimal degrees)	Altitude (m.a.s.l.)	$\delta^{2}H$ (‰) VSMOW	$\delta^{18}O$ (‰) VSMOW	d-excess (‰)	$\delta^{30}Si$ (‰) NBS-28	2SD	$\delta^{29}Si$ (‰) NBS-28	2SD	DSi conc.	
														(mg/L)	(µM)
White Nile	1	Bujuku River, Rwenzori Mountains, Uganda	Oct-10	0.3581	29.9718	2552	-18.4	-4.7	+19.6						
	2	River Mubuku, Rwenzori Mountains, Uganda	Oct-10	0.3581	29.9718	2552	-17.0	-4.6	+19.6						
	3	River Mubuku, Rwenzori Mountains, Uganda	Oct-10	0.3436	30.0399	1608	-11.4	-3.9	+19.6	+0.99	0.15	+0.46	0.14	5.7	203
	4	River Ishasha, Uganda	Oct-10	-0.6157	29.6578	934	-2.8	-2.4	+16.3	+0.98	0.15	+0.60	0.14	5.6	199
	5	River Ntungwe, Uganda	Oct-10	-0.5667	29.7235	938	-0.6	-1.8	+13.8	+1.73	0.20	+0.87	0.16	12.0	427
	6	Mpanga River, Uganda	Oct-10	0.0832	30.3224	1201	+1.3	-1.5	+13.2						
	7	Lake Mahoma, Rwenzori Mountains, Uganda	Oct-10	0.3455	29.9684	2880	+0.5	-1.5	+12.4	+0.48	0.12	+0.08	0.09	1.1	39
	8	River Nkusi, Uganda	Nov-10	1.1301	30.9946	1029	+2.7	-1.3	+12.8						
	9	River Kagera, Uganda	Oct-10	-0.9393	31.7632	1139	-0.1	-1.0	+7.7	+2.14	0.21	+1.10	0.16	7.1	253
	10	River Kafu, Uganda	Nov-10	1.5454	32.0389	1045	+7.7	-0.1	+8.7						
	11	River Semliki, Uganda-Congo	Oct-10	1.0287	30.5283	653	+10.6	+0.2	+9.2	+1.57	0.19	+0.85	0.20	8.9	317
	12	Kazinga Channel, Uganda	Oct-10	-0.1883	29.9073	918	+15.5	+1.3	+4.8	+1.74	0.19	+0.85	0.24	10.2	363
	13	White Nile, Khartoum, Sudan	Dec-10	15.6141	32.4937	391	+22.1	+2.2	+4.4	+2.36	0.16	+1.21	0.14	6.0	214
	14	Albert Nile, Uganda	Nov-10	2.2859	31.3727	633	+25.3	+3.3	-0.9	+2.28	0.20	+1.20	0.09	2.9	103
	15	Victoria Nile Delta, Uganda	Nov-10	2.2509	31.3834	628	+24.6	+3.3	-2.0	+1.88	0.09	+1.12	0.04	3.3	117
	16	Lake Albert (north), Uganda-Congo	Nov-10	2.2208	31.3316	631	+25.3	+3.4	-2.1						
	17	Murchison Falls, Victoria Nile, Uganda	Nov-10	2.2749	31.6752	635	+26.3	+3.5	-1.6						
	18	Victoria Nile, Bujagali Falls, Uganda	Nov-10	0.4831	33.1630	1112	+26.1	+3.5	-2.3	+2.02	0.15	+0.97	0.10	1.5	53
	19	Outflow from Lake Victoria (Jinja), Uganda	Nov-10	0.4208	33.1964	1135	+25.9	+3.7	-3.5	+2.36	0.12	+1.05	0.08	1.1	39
	20	Lake Albert (south), Uganda-Congo	Oct-10	1.0440	30.5294	618	+31.7	+4.1	-1.0	+2.13	0.21	+0.93	0.10	2.8	100
Blue Nil Nana Atbara	25	Ribb River, east Lake Tana, Ethiopia	Oct-10	11.9937	37.7109	1799	-4.9	-2.4	+13.9	+1.82	0.18	+1.00	0.17	8.8	313
	26	Gish Abay, Ethiopia	Oct-10	10.9716	37.1991	2721	-0.6	-2.3	+18.2						
	27	Gilgel Abay, Ethiopia	Oct-10	11.3648	37.0341	1875	+0.2	-2.2	+17.5						
	28	Chimba, Gilgel Abay, Ethiopia	Oct-10	11.7060	37.1673	1809	+0.0	-1.9	+14.9	+1.53	0.16	+0.81	0.14	7.4	263
	29	Alata River, Ethiopia	Oct-10	11.4963	37.5909	1617	+0.1	-1.6	+12.9						
	30	Gumara River, east Lake Tana, Ethiopia	Oct-10	11.8393	37.6354	1795	+2.3	-1.5	+14.5						
	31	River Zarima, Ethiopia	Oct-10	13.3419	37.8788	1220	+4.3	-1.5	+16.3	+1.22	0.23	+0.68	0.16	18.9	673
	32	River Tekezé, Ethiopia	Oct-10	13.7337	38.1878	900	-0.0	-1.4	+11.3	+1.89	0.16	+1.05	0.15	9.9	352
	33	River Magech, north Lake Tana, Ethiopia	Oct-10	12.4872	37.4475	1882	+5.9	-0.6	+10.7	+1.66	0.20	+0.85	0.16	16.0	570
	34	Blue Nile, Khartoum, Sudan	Dec-10	15.6139	32.5325	409	+16.3	+1.1	+7.4	+2.50	0.20	+1.31	0.15	7.3	260
	35	Tis Issat Falls, Blue Nile, Ethiopia	Oct-10	11.4904	37.5855	1642	+16.5	+1.1	+7.4	+2.23	0.18	+1.06	0.17	4.9	174
	36	River Atbara, Atbara, Sudan	Dec-10	17.6778	33.9762	353	+20.8	+2.5	+1.0	+3.23	0.19	+1.78	0.17	8.8	313
	37	Blue Nile, Bahir Dar, Ethiopia	Oct-10	11.6059	37.4074	1804	+26.7	+3.0	+2.6						
Main Nile	38	Main Nile (Lake Nasser), Wadi Halfa, Sudan	Dec-10	21.8079	31.3156	170	+7.5	-0.0	+7.8						
	39	Main Nile, Dongola, Sudan	Dec-10	19.1811	30.4874	223	+10.0	+0.2	+8.6	+2.12	0.20	+1.06	0.16	6.3	224
	40	Main Nile, Karima, Sudan	Dec-10	18.4957	31.8091	258	+10.0	+0.1	+8.9						
	41	Main Nile, Atbara, Sudan	Dec-10	17.6620	33.9745	357	+20.7	+2.1	+4.2	+2.62	0.22	+1.33	0.16	5.8	207
	42	Main Nile, Khartoum, Sudan	Dec-10	15.6473	32.5086	409	+22.2	+2.1	+5.3						
	43	Main Nile, Aswan, Egypt	Dec-10	24.0829	32.8869	77	+24.8	+3.4	-2.1						
	44	Bahr Yusuf, Faiyum, Egypt	Nov-10	29.3084	30.8450	8	+25.6	+3.4	-1.6						
	45	Main Nile, Cairo, Egypt	Nov-10	30.0430	31.2276	4	+26.2	+3.6	-2.7					0.9	32
	46	Main Nile, Luxor, Egypt	Dec-10	25.7032	32.3847	82	+26.7	+3.5	-1.6	+3.45	0.24	+1.89	0.12	2.9	103
	47	Main Nile (Lake Nasser), Aswan, Egypt	Dec-10	23.9703	32.8962	152	+27.0	+3.7	-2.3	+3.45	0.21	+1.85	0.10	3.4	121
	48	Lake Qarun, Faiyum (south-east), Egypt	Nov-10	29.4694	30.7696	-51	+41.7	+6.7	-11.7						
	49	Lake Qarun, Faiyum (south-west), Egypt	Nov-10	29.4694	30.7696	-51	+47.7	+8.0	-16.5						

Table 1. cont.

	Site No.	Sample site name and location	Dry season												
			Date (month -year)	Latitude (decimal degrees)	Longitude (decimal degrees)	Altitude (m.a.s.l.)	δ^2H (‰) VSMOW	$\delta^{18}O$ (‰) VSMOW	d-excess (‰)	$\delta^{30}Si$ (‰) NBS-28	2SD	$\delta^{29}Si$ (‰) NBS-28	2SD	DSi conc. (mg/L)	DSi conc. (µM)
White Nile	11	River Semliki, Uganda-Congo	Jun-09	1.0630	30.2269	636	+19.0	+1.4	+7.7	+1.74	0.15	+0.91	0.14	6.9	246
	12	Kazinga Channel, Uganda	Jun-09	-0.1849	29.9055	917	+19.2	+1.9	+3.9	+1.54	0.20	+0.74	0.16	10.7	381
	13	White Nile, Khartoum, Sudan	May-11	15.6141	32.4937	391	+47.5	+7.0	-8.3	+1.70	0.11	+0.81	0.06	3.8	135
	14	Albert Nile, Uganda	May-09	2.3913	31.4769	614	+33.9	+4.5	-1.9	+2.51	0.14	+1.25	0.08	1.2	43
	15	Victoria Nile Delta, Uganda	May-09	2.2449	31.3913	618	+29.2	+4.0	-2.8	+2.16	0.11	+1.27	0.13	2.1	75
	16	Lake Albert (north), Uganda-Congo	May-09	2.2601	31.3486	614	+29.6	+4.0	-2.4						
	17	Murchison Falls, Victoria Nile, Uganda	May-09	2.2735	31.6693	623	+29.3	+4.0	-2.9						
	18	Victoria Nile, Bujagali Falls, Uganda	Jun-09	0.4610	33.1755	1126	+29.0	+3.6	+0.4						
	19	Outflow from Lake Victoria (Jinja), Uganda	Jun-09	0.4208	33.1963	1137	+29.1	+3.5	+1.2					0.2	7
	20	Lake Albert (south), Uganda-Congo	Jun-09	1.0309	30.5076	620	+34.8	+4.7	-3.1	+2.66	0.12	+1.18	0.09	1.2	43
	21	Lake Edward, Uganda	Jun-09	-0.2093	29.8856	911	+19.3	+1.9	+4.3						
	22	Ssese Islands, Lake Victoria, Uganda	Jun-09	-0.2554	32.0386	1133	+26.0	+3.1	+1.0						
	23	Lake Victoria, Entebbe, Uganda	Jun-09	0.0560	32.4814	1134	+26.8	+3.1	+1.7						
	24	Paraa, Victoria Nile, Uganda	May-09	2.2864	31.5747	622	+29.0	+4.0	-3.1						
Blue Nile and Atbara	25	Ribb River, east Lake Tana, Ethiopia	May-09	11.9943	37.7130	1794	+47.3	+8.8	-22.7	+3.51	0.14	+1.92	0.13	3.3	117
	28	Chimba, Gilgel Abay, Ethiopia	May-09	11.7081	37.1680	1808	+15.5	+1.4	+4.1	+1.74	0.07	+0.88	0.03	10.9	388
	29	Alata River, Ethiopia	May-09	11.4929	37.5902	1647	+10.4	+0.6	+5.3						
	30	Gumara River, east Lake Tana, Ethiopia	May-09	11.8379	37.6359	1795	+33.7	+5.6	-11.3						
	34	Blue Nile, Khartoum, Sudan	May-11	15.6139	32.5325	409	+32.1	+4.2	-1.8	+3.22	0.16	+1.70	0.14	5.7	203
	35	Tis Issat Falls, Blue Nile, Ethiopia	May-09	11.4904	37.5855	1642	+37.9	+5.1	-3.1	+3.31	0.24	+1.84	0.17	3.7	132
	36	River Atbara, Atbara, Sudan	Apr-11	17.6778	33.9762	353	+15.3	+1.6	+2.4	+3.41	0.19	+1.80	0.16	5.1	182
	37	Blue Nile, Bahir Dar, Ethiopia	May-09	11.6050	37.4079	1788	+37.3	+5.1	-3.2						
Main Nile	38	Main Nile (Lake Nasser), Wadi Halfa, Sudan	Apr-11	22.0218	31.3393	178	+16.8	+1.3	+6.2						
	39	Main Nile, Dongola, Sudan	Apr-11	19.1811	30.4874	223	+26.3	+2.8	+3.9	+2.83	0.20	+1.39	0.16	4.6	164
	40	Main Nile, Karima, Sudan	Apr-11	18.4957	31.8091	258	+27.0	+2.9	+4.1						
	41	Main Nile, Atbara, Sudan	Apr-11	17.6620	33.9745	357	+44.8	+6.6	-8.0	+2.14	0.26	+1.29	0.14	4.0	142
	42	Main Nile, Khartoum, Sudan	May-11	15.6569	32.5103	377	+48.0	+7.1	-8.9						
	43	Main Nile, Aswan, Egypt	Apr-11	24.0888	32.8922	81	+21.1	+2.1	+4.1						
	44	Bahr Yusuf, Faiyum, Egypt	Apr-11	29.3084	30.8451	20	+24.2	+2.8	+1.9						
	45	Main Nile, Cairo, Egypt	Apr-11	30.0420	31.2269	8	+24.4	+2.8	+2.3	+4.66	0.15	+2.26	0.10	1.1	39
	46	Main Nile, Luxor, Egypt	Apr-11	25.7028	32.6370	67	+22.2	+2.3	+3.8	+3.63	0.20	+1.96	0.11	2.6	93
	47	Main Nile (Lake Nasser), Aswan, Egypt	Apr-11	23.9702	32.8963	152	+21.6	+2.1	+4.7	+3.79	0.21	+2.01	0.10	2.7	96
	48	Lake Qarun, Faiyum (south-east), Egypt	Apr-11	29.4683	30.7789	-44	+48.6	+7.6	-12.4						
	50	Lake Qarun, Faiyum (west), Egypt	Apr-11	29.4541	30.4003	-46	+53.9	+8.8	-16.6						

Table 2.

Silicon isotope data for analysed Diatomite reference material.

	28Si (V)	24Mg (V)	$^{30}Si/^{28}Si$	$^{25}Mg/^{24}Mg$	$\delta^{30}Si$ (‰) NBS-28	2SD	$\delta^{29}Si$ (‰) NBS-28	2SD
Diatomite	7.73	1.37	0.037640	0.135899	1.44	0.19	0.80	0.17
Diatomite	5.73	1.40	0.037638	0.135892	1.49	0.18	0.79	0.17
Diatomite	4.15	1.29	0.037590	0.135788	1.20	0.20	0.69	0.08
Diatomite	4.05	1.32	0.037569	0.135758	1.11	0.22	0.50	0.11
Diatomite	4.03	1.23	0.037574	0.135755	1.24	0.19	0.68	0.11
Diatomite	5.04	1.38	0.037583	0.135767	1.19	0.12	0.54	0.07
Diatomite	5.07	1.26	0.037586	0.135771	1.24	0.10	0.78	0.12
Diatomite	7.63	1.36	0.037571	0.135759	1.16	0.14	0.60	0.13
Diatomite	5.27	1.31	0.037565	0.135736	1.26	0.13	0.69	0.13
Diatomite	2.00	1.33	0.037584	0.135798	1.28	0.14	0.57	0.09
Diatomite	2.34	1.40	0.037527	0.135660	1.40	0.19	0.64	0.24
Diatomite	7.66	1.45	0.037555	0.135718	1.43	0.19	0.60	0.24
Diatomite	7.45	1.41	0.037564	0.135740	1.45	0.19	0.74	0.25
Diatomite	2.83	1.49	0.037657	0.135954	1.28	0.17	0.63	0.14
Diatomite	9.80	1.53	0.037620	0.135885	1.25	0.16	0.63	0.14
Diatomite	14.38	1.52	0.037606	0.135845	1.33	0.17	0.65	0.15
Diatomite	5.33	0.84	0.037610	0.135876	1.02	0.21	0.44	0.16
Diatomite	7.70	1.32	0.037477	0.135572	1.26	0.20	0.65	0.15
Diatomite	5.67	1.32	0.037503	0.135645	1.12	0.21	0.52	0.16
Diatomite	8.06	1.27	0.037513	0.135645	1.40	0.20	0.67	0.15

Table 3.

Regression results for δ^2H and $\delta^{18}O$ of surface water samples in Fig. 3.

	Regression equation	R^2	Mean $\delta^{18}O$	1 S.D.	δ^2H	1 S.D.	n
Wet season							
River Nile (all data)	$\delta^2H = 5.09 \cdot \delta^{18}O + 8.78$	0.989	+0.8	± 2.9	+12.7	± 14.8	45
White Nile	$\delta^2H = 5.27 \cdot \delta^{18}O + 8.22$	0.992	+0.3	± 3.0	+9.8	± 15.7	20
Blue Nile	$\delta^2H = 5.22 \cdot \delta^{18}O + 9.80$	0.973	-0.6	± 1.9	+6.7	± 9.9	13
Main Nile	$\delta^2H = 4.83 \cdot \delta^{18}O + 9.41$	0.992	+3.1	± 2.5	+24.2	± 12.0	12
Dry season							
River Nile (all data)	$\delta^2H = 4.95 \cdot \delta^{18}O + 10.43$	0.966	+3.9	± 2.2	+29.7	± 10.9	34
White Nile	$\delta^2H = 5.23 \cdot \delta^{18}O + 9.75$	0.976	+3.6	± 1.4	+28.7	± 7.4	14
Blue Nile	$\delta^2H = 4.76 \cdot \delta^{18}O + 9.35$	0.947	+4.1	± 2.7	+28.7	± 13.3	8
Main Nile	$\delta^2H = 5.00 \cdot \delta^{18}O + 11.06$	0.994	+4.1	± 2.6	+31.6	± 13.1	12

Fig. 1. Location of the River Nile and sampling sites within the Nile basin. Sampled sites are numbered and correspond to those listed in Table 1.

Fig. 2. General characteristics of the Nile basin. (a) Simplified geology of the Nile basin (modified after Furon (1958)). (b) Schematic of the low-level mean wind directions for tropical Africa in the boreal summer (June–August) and the austral summer (December–February), based on NCEP reanalysis 925 hPa mean winds and work by Nicholson (1996). The approximate positions of the Intertropical Convergence Zone (ITCZ) and the Congo Air Boundary (CAB) are indicated (modified after Levin *et al.* (2009)). (c) Seasonal distribution of African rainfall between 10^0S and 32^0N as a function of month and latitude (25ºE to 50ºE) (modified after Nicholson, 2009). (d) Simplified vegetation map of northern Africa including the River Nile, showing the distribution of the major floristic regions (redrawn from White, 1983).

Fig. 3. δ^2H and $\delta^{18}O$ of surface water samples for (a) the Nile basin, and for the major individual tributaries, (b) White Nile, (c) Blue Nile and (d) Main Nile. Samples collected during the wet season (circles) and dry season (squares) are plotted. The African Meteoric Water Line (AMWL) (solid line: $\delta^2H=7.4\cdot\delta^{18}O+10.1$) (Cohen *et al.*, 1997), wet- (dotted line) and dry-season (dashed line) local evaporative lines are plotted for reference. For sample numbers, see Table 1. Corresponding regression results can be found in Table 3.

Fig. 4. $\delta^{18}O$ versus latitude (a) and altitude (b). Wet season (closed symbols) and dry season (open symbols) samples are plotted for the White Nile (squares), Blue Nile (circles) and Main Nile (triangles). Seasonal trends are identified with regression lines; waters were more enriched during the dry season (dashed line; $\delta^{18}O = 0.03\cdot\text{Latitude}+3.49$, $r_s = 0.076$, $p = 0.338$; $\delta^{18}O = 2E\text{-}05\cdot\text{Altitude}+3.88$, $r_s = 0.015$, $p = 0.468$) than the wet season (dotted line; $\delta^{18}O = 0.14\cdot\text{Latitude}-0.68$, $r_s = 0.465$, $p < 0.001$; $\delta^{18}O = -0.003\cdot\text{Altitude}+3.36$, $r_s = -0.724$, $p < 0.001$). Progressive northwards and downstream enrichment of $\delta^{18}O$ was only significant during the wet-season. For sample numbers, see Table 1.

Fig. 5. Seasonal variations of d-excess for the River Nile with latitude (a) and altitude (b). Wet-season (closed symbols) and dry-season (open symbols) samples are plotted from the White Nile (squares), Blue Nile (circles) and Main Nile (triangles). Horizontal line at +10‰ represents the GMWL. Circled samples are referred to in the text. For numbered samples see Table 1.

Fig. 6. Si concentration versus latitude. Si concentrations are presented in both mg/L (left y-axis) and µM (right y-axis) units. Wet season (closed symbols) and dry season (open symbols) samples are plotted for the White Nile (squares), Blue Nile (circles) and Main Nile (triangles). Seasonal trends are identified with individual regression lines for the White Nile (left-hand side) and the Blue Nile, Atbara and Main Nile (right-hand side) during the wet season (dotted line) and dry season (dashed line) to account for varying geology. White Nile wet season (dotted line; DSi = -1.67·Latitude+6.00, R^2 = 0.218, p = 0.063) and dry season (dashed line; DSi = -2.29·Latitude+6.38, R^2 = 0.308, p = 0.127). Blue Nile, Atbara and Main Nile wet season (dotted line; DSi = $41.57 \cdot \exp^{-0.11 \cdot \text{Latitude}}$, R^2 = 0.705, p < 0.001) and dry season (dashed line; DSi = $14.33 \cdot \exp^{-0.07 \cdot \text{Latitude}}$, R^2 = 0.592, p = 0.004). Sample site 13 (White Nile, Khartoum) has been omitted from the White Nile regression as its composition suggests that it may have been influenced by surface water, groundwater or sediments ultimately derived from the Blue Nile, although there are too few data to draw any firm conclusions at this point. For sample numbers, see Table 1.

Fig. 7. δ^{30}Si versus latitude. Wet season (closed symbols) and dry season (open symbols) samples are plotted from the White Nile (squares), Blue Nile (circles) and Main Nile (triangles). Seasonal trends are identified with curvilinear regression lines for the wet season (dotted line; $\delta^{30}Si = 0.004 \cdot (\text{Latitude})^2 - 0.03 \cdot (\text{Latitude}) + 1.67$, R^2 = 0.522, p < 0.001) and for the dry season (dashed line; $\delta^{30}Si = 0.002 \cdot (\text{Latitude})^2 + 0.003 \cdot (\text{Latitude}) + 2.13$, R^2 = 0.554, p < 0.001). For sample numbers, see Table 1.

Fig. 8. δ^{30}Si versus Si concentration. Si concentrations are presented in both mg/L (bottom x-axis) and µM (top x-axis) units. Wet-season (closed symbols) and dry-season (open symbols) samples are plotted from the White Nile (squares), Blue Nile (circles) and Main Nile (triangles). Seasonal trends are identified with regression lines for the wet season (dotted line; $\delta^{30}Si = -0.001 \cdot DSi + 2.28$, R^2 = 0.058, p = 0.245) and for the dry season (dashed line; $\delta^{30}Si = 3.56 \cdot \exp^{-0.007 \cdot DSi}$, R^2 = 0.371, p = 0.012). For sample numbers, see Table 1.

Fig. 9. δ^{30}Si versus δ^{18}O. Wet season (closed symbols) and dry season (open symbols) samples are plotted for the White Nile (squares), Blue Nile (circles) and Main Nile (triangles). Seasonal trends are identified with regression lines for the wet season (dotted line; $\delta^{30}Si = 0.22 \cdot \delta^{18}O + 1.86$, R^2 = 0.517, p < 0.001) and for the dry season (dashed line; $\delta^{30}Si = 0.003 \cdot \delta^{18}O + 2.80$, R^2 = 5E-05, p = 0.980). For sample numbers, see Table 1.

Fig. 1

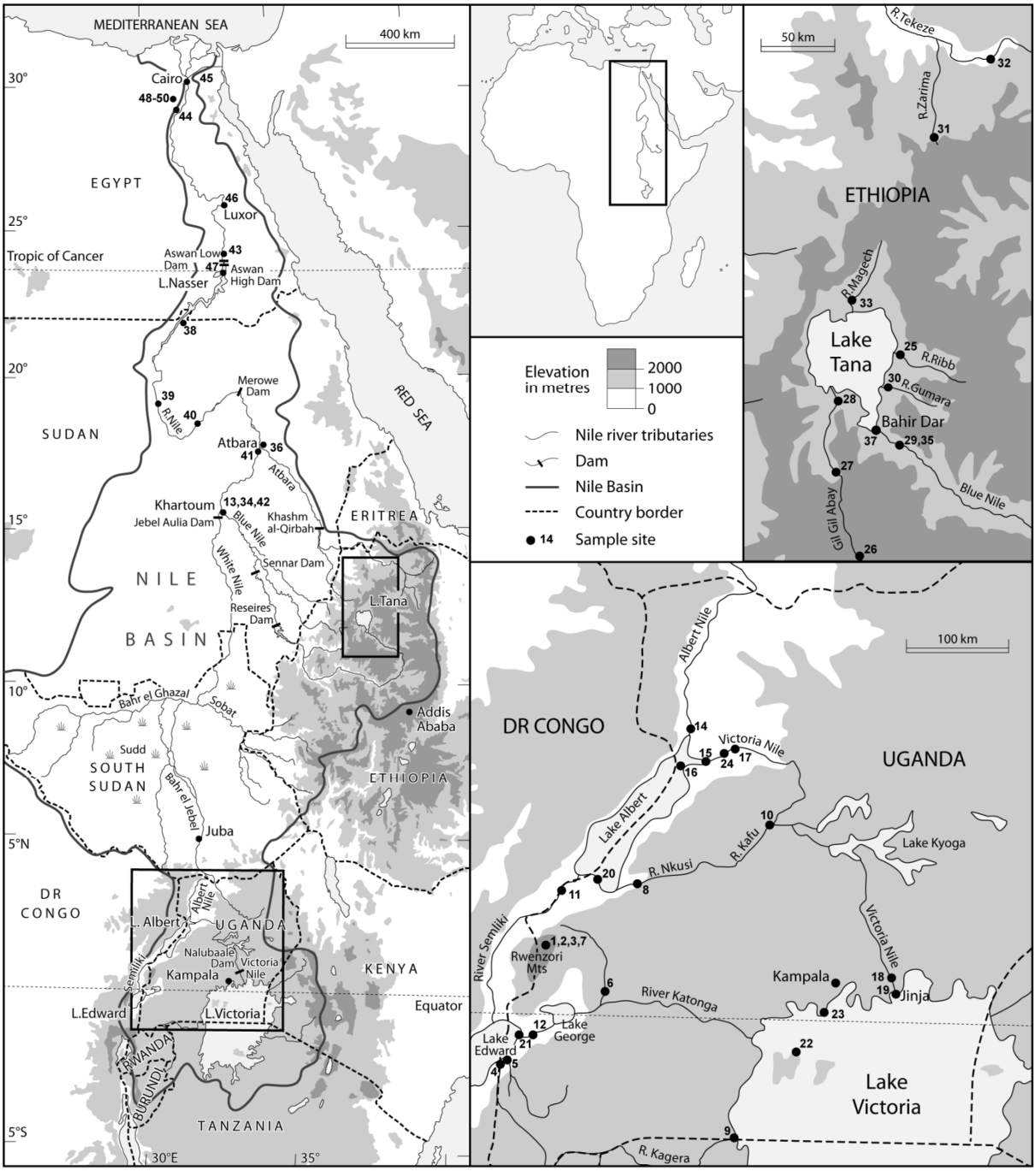
MEDITERRANEAN SEA
400 km
30°
25°
20°
15°
10°
5°N
5°S
30°E
35°
Tropic of Cancer
Equator
EGYPT
SUDAN
SOUTH SUDAN
ERITREA
ETHIOPIA
KENYA
UGANDA
DR CONGO
RWANDA
BURUNDI
TANZANIA
RED SEA
NILE BASIN
Cairo
45
48-50
44
46
Luxor
Aswan Low Dam
43
47
Aswan High Dam
L.Nasser
38
Merowe Dam
39
R.Nile
40
Atbara
36
41
Atbara
Khartoum
13,34,42
Jebel Aulia Dam
Blue Nile
Khashm al-Qirbah
White Nile
Sennar Dam
Reseires Dam
L.Tana
Addis Ababa
Bahr el Ghazal
Sobat
Sudd
Bahr el Jebel
Juba
DR CONGO
Albert Nile
L. Albert
Nalubaale Dam
Victoria Nile
Kampala
Semliki
L.Edward
L.Victoria
Elevation in metres
2000
1000
0
Nile river tributaries
Dam
Nile Basin
Country border
14
Sample site
50 km
R.Tekeze
32
R.Zarima
31
ETHIOPIA
R.Magech
33
Lake Tana
25
R.Ribb
30
R.Gumara
28
Bahir Dar
37
29,35
27
Blue Nile
Gil Gil Abay
26
100 km
Albert Nile
DR CONGO
14
Victoria Nile
15
24
17
16
UGANDA
Lake Albert
10
R. Kafu
Lake Kyoga
20
R. Nkusi
8
11
River Semliki
1,2,3,7
Rwenzori Mts
6
River Katonga
Victoria Nile
Kampala
18
19
Jinja
23
12
Lake George
21
Lake Edward
5
4
22
Lake Victoria
9
R. Kagera

Fig.2

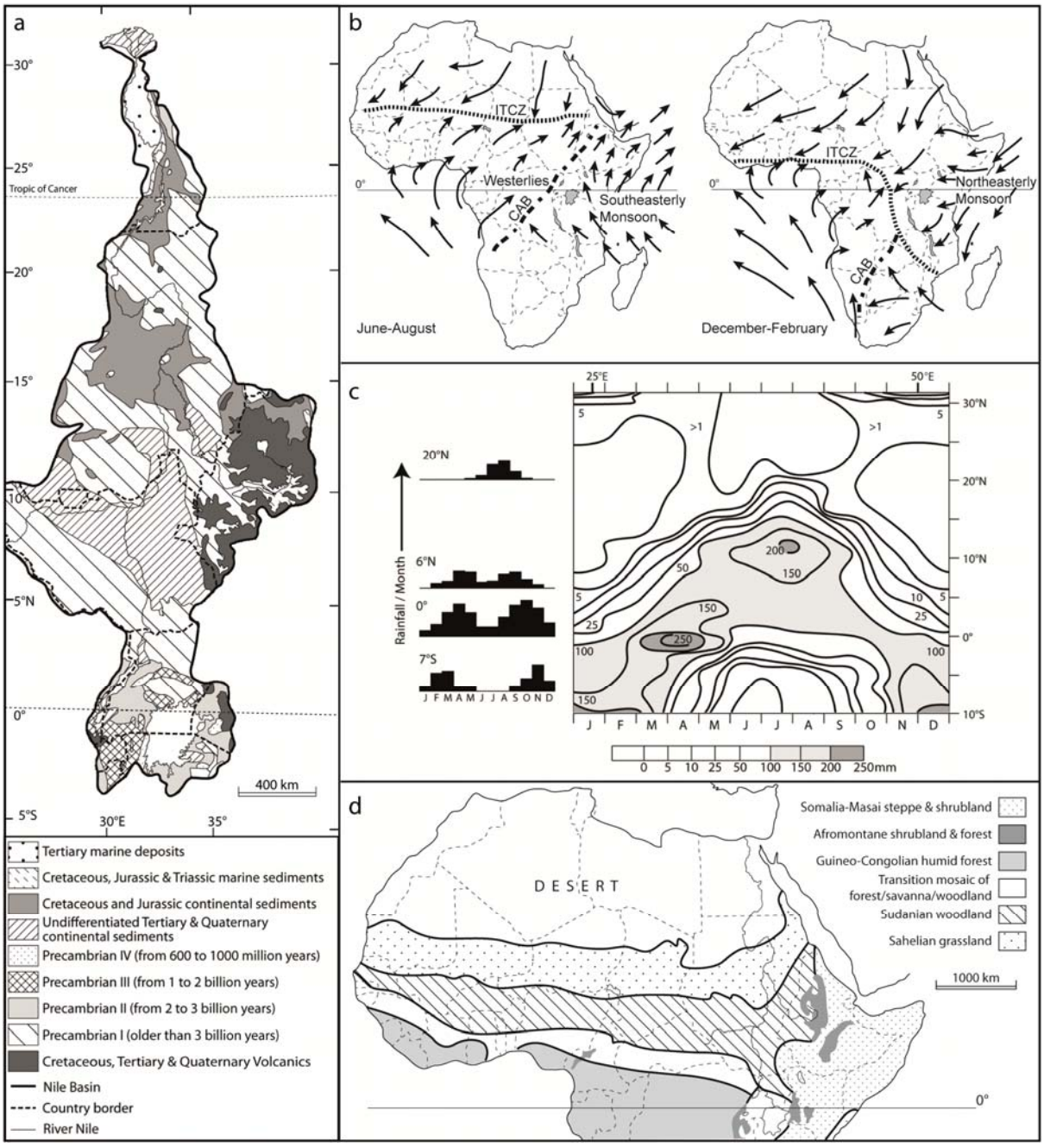
a
30°
25°
Tropic of Cancer
20°
15°
10°
5°N
0°
5°S
30°E
35°
400 km
Tertiary marine deposits
Cretaceous, Jurassic & Triassic marine sediments
Cretaceous and Jurassic continental sediments
Undifferentiated Tertiary & Quaternary continental sediments
Precambrian IV (from 600 to 1000 million years)
Precambrian III (from 1 to 2 billion years)
Precambrian II (from 2 to 3 billion years)
Precambrian I (older than 3 billion years)
Cretaceous, Tertiary & Quaternary Volcanics
Nile Basin
Country border
River Nile
b
ITCZ
Westerlies
Southeasterly Monsoon
CAB
June-August
ITCZ
Northeasterly Monsoon
CAB
December-February
c
20°N
6°N
0°
7°S
J F M A M J J A S O N D
Rainfall / Month
25°E
50°E
30°N
20°N
10°N
0°
10°S
J F M A M J J A S O N D
0 5 10 25 50 100 150 200 250mm
d
DESERT
Somalia-Masai steppe & shrubland
Afromontane shrubland & forest
Guineo-Congolian humid forest
Transition mosaic of forest/savanna/woodland
Sudanian woodland
Sahelian grassland
1000 km
0°

Fig.3

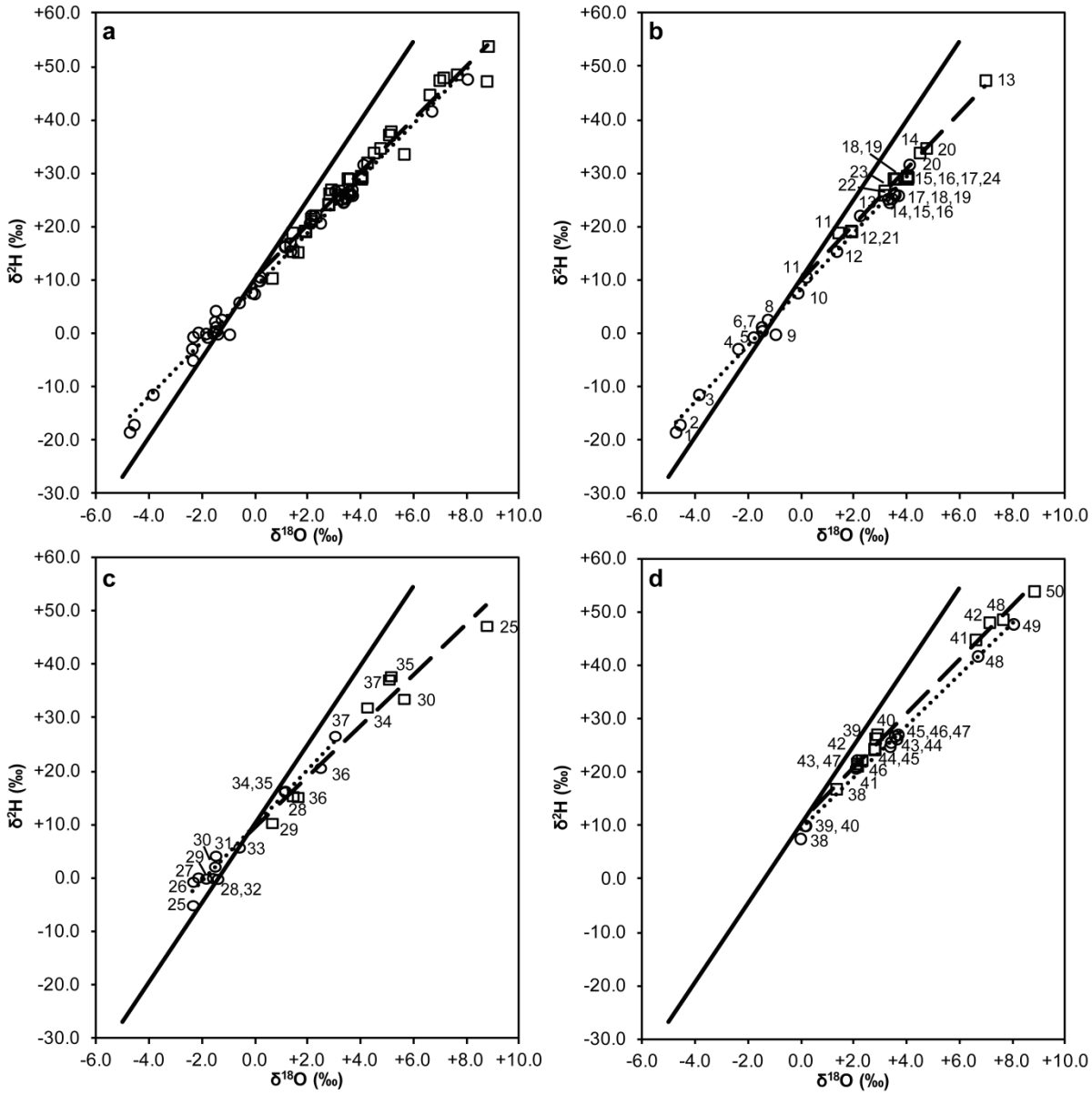
a
b
c
d
δ²H (‰)
δ¹⁸O (‰)
+60.0
+50.0
+40.0
+30.0
+20.0
+10.0
0.0
-10.0
-20.0
-30.0
-6.0
-4.0
-2.0
0.0
+2.0
+4.0
+6.0
+8.0
+10.0

Fig.4

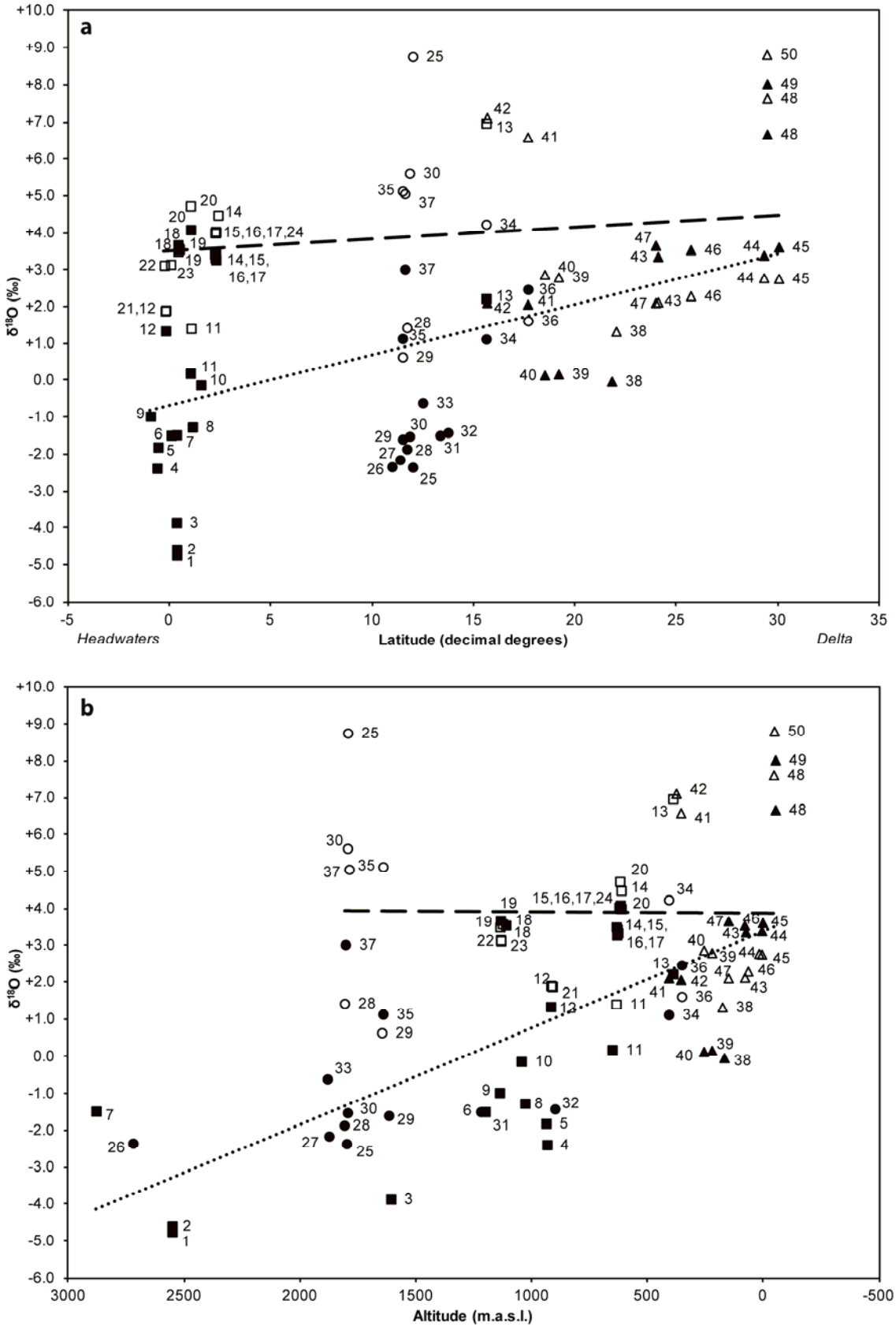
a
b
δ18O (‰)
Latitude (decimal degrees)
Headwaters
Delta
Altitude (m.a.s.l.)

Fig.5

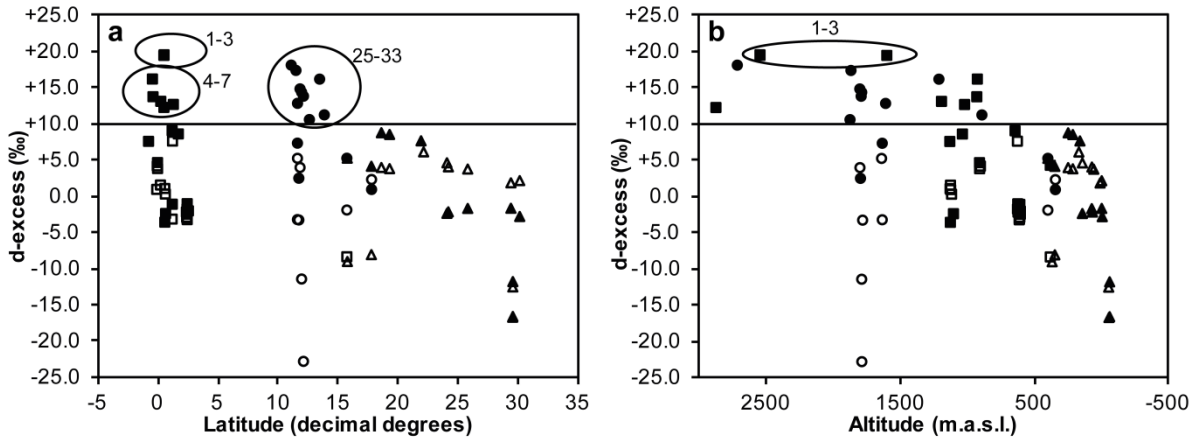
a
1-3
4-7
25-33
d-excess (‰)
+25.0
+20.0
+15.0
+10.0
+5.0
0.0
-5.0
-10.0
-15.0
-20.0
-25.0
-5
0
5
10
15
20
25
30
35
Latitude (decimal degrees)
b
1-3
d-excess (‰)
2500
1500
500
-500
Altitude (m.a.s.l.)

Fig.6

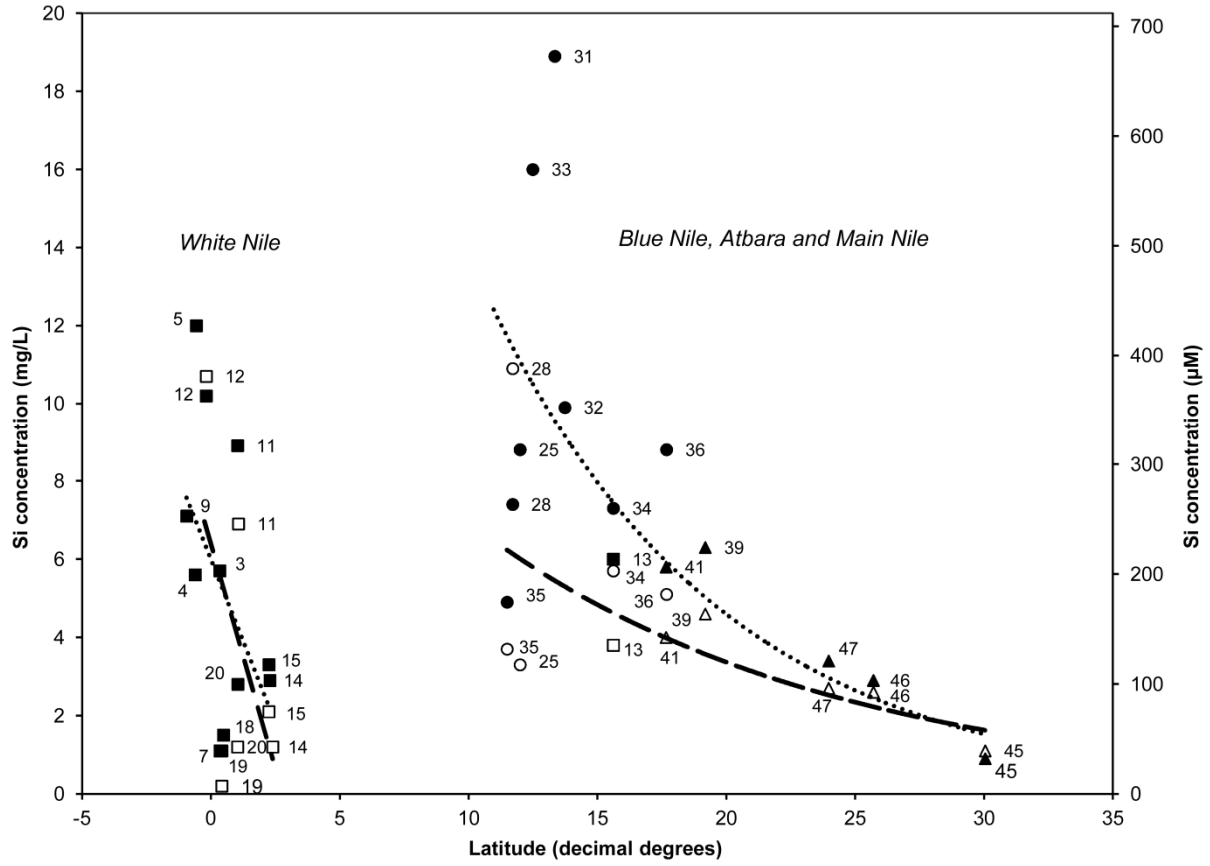
White Nile
Blue Nile, Atbara and Main Nile
Si concentration (mg/L)
Si concentration (µM)
Latitude (decimal degrees)

Fig.7

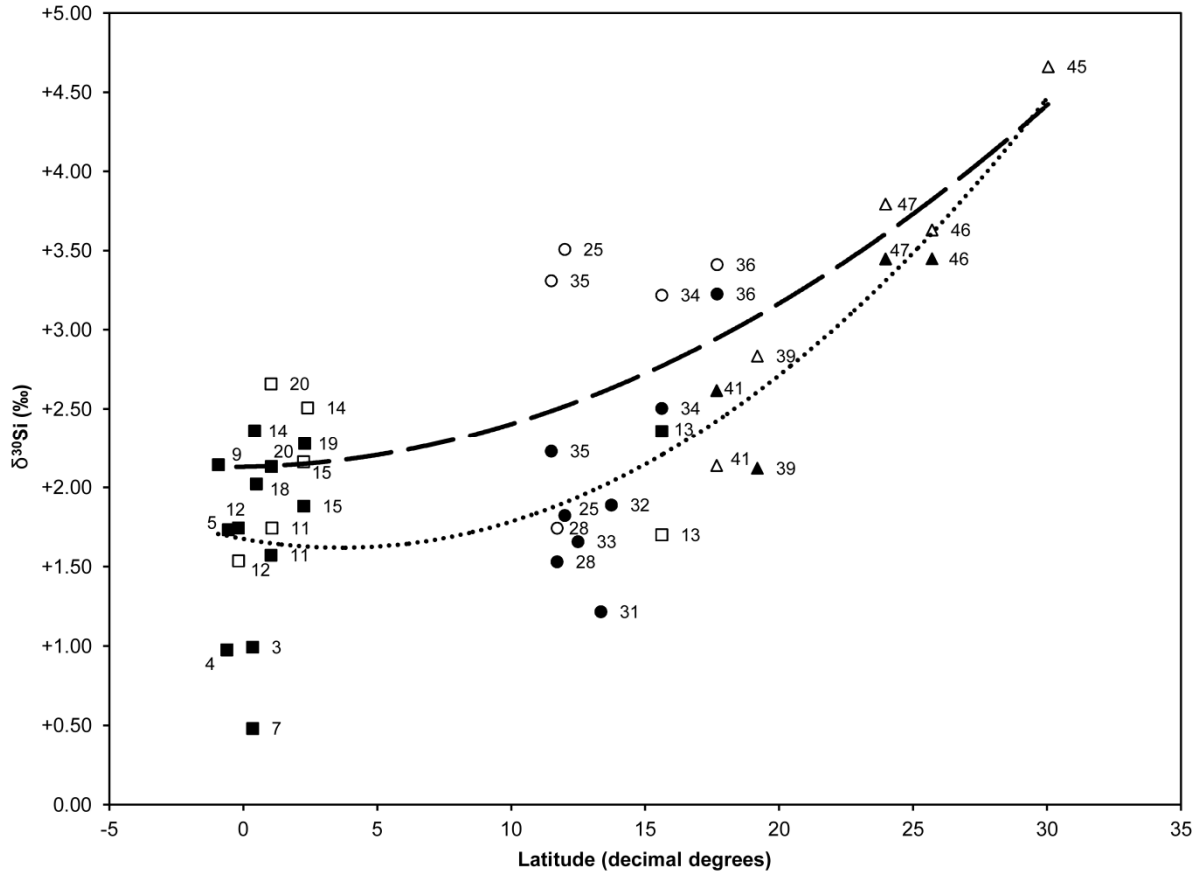
δ30Si (‰)
Latitude (decimal degrees)
+5.00
+4.50
+4.00
+3.50
+3.00
+2.50
+2.00
+1.50
+1.00
+0.50
0.00
-5
0
5
10
15
20
25
30
35

Fig.8

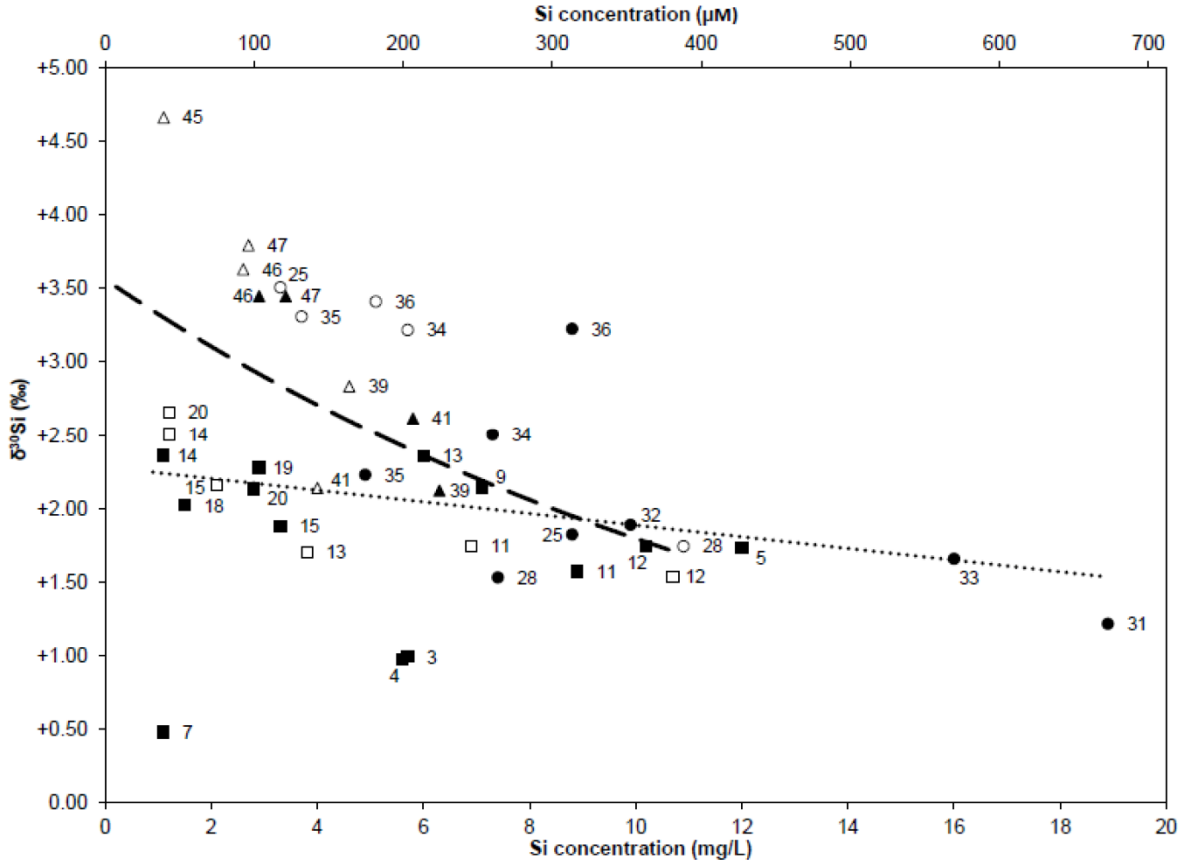
Si concentration (μM)
0
100
200
300
400
500
600
700
+5.00
+4.50
+4.00
+3.50
+3.00
+2.50
+2.00
+1.50
+1.00
+0.50
0.00
δ30Si (‰)
0
2
4
6
8
10
12
14
16
18
20
Si concentration (mg/L)

Fig.9

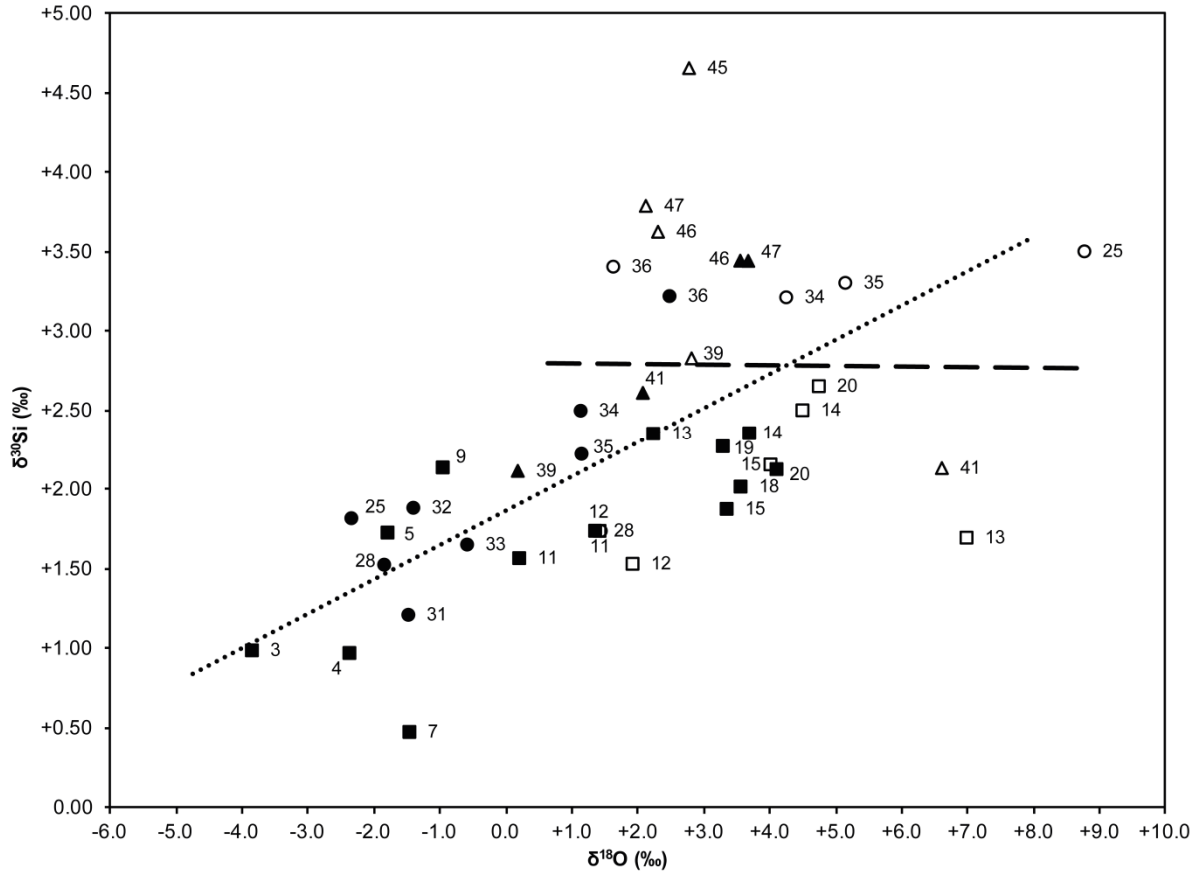
+5.00
+4.50
+4.00
+3.50
+3.00
+2.50
+2.00
+1.50
+1.00
+0.50
0.00
δ30Si (‰)
-6.0
-5.0
-4.0
-3.0
-2.0
-1.0
0.0
+1.0
+2.0
+3.0
+4.0
+5.0
+6.0
+7.0
+8.0
+9.0
+10.0
δ18O (‰)